

Permian–polysulphide–siderite–barite–haematite deposit Rude in Samoborska Gora Mts., Zagorje–Mid–Transdanubian zone of the Internal Dinarides



Ladislav A. Palinkaš¹, Sibila Borojević Šoštarić¹, Sabina Strmić Palinkaš¹, Walter Prochaska², Jorge Spangenberg³, Stela Cuna⁴ and †Boris Šinkovec⁵

¹ Faculty of Science, University of Zagreb, Horvatovac 95, HR-10000 Zagreb, Croatia; (lpalinkas@geol.pmf.hr; phone: +385-1-465-971; fax: +385-1-4605-988)

² Institut für Geowissenschaften, Montanuniversität, Peter-Tunner-Strasse 5, A-8700 Leoben, Austria

³ Institute of Mineralogy and Geochemistry, University of Lausanne, BFSH-2, CH-1015 Lausanne, Switzerland

⁴ National Institute for Research and Development of Isotopic and Molecular Technologies, 65–103 Donath, RO-400293 Cluj-Napoca, Romania

⁵ Faculty of Mining, Geology and Petroleum Engineering, University of Zagreb, Croatia

doi: 104154/gc.2010.06

Geologia Croatica

ABSTRACT

Samoborska Gora Mts. is situated within the westernmost part of the Zagorje–Mid–Transdanubian zone of the Internal Dinarides. The Samoborska Gora Mts. predominantly consists of Permian unmetamorphosed siliciclastic sediments and evaporites, overlain by Lower Triassic sediments. Rude mineralisation is hosted by Permian siliciclastic sediments, below gypsum and anhydrite strata. The central part of the deposit consists of a 1.5 km long stratabound mineralisation, grading laterally into ferruginous sandstone and protruding vertically into a gypsum–anhydrite layer. Siderite–polysulphide–barite–quartz veins are located below the stratabound mineralisation. The stratiform part of the deposit is situated above the stratabound and consists of haematite layer with barite concretions and veinlets. Late stage galena–barite veins overprint earlier types of mineralisation.

The Rude ore deposit was generated by predominantly NaCl ± CaCl₂–H₂O solutions. Detrital quartz from stratiform mineralisation contains fluid inclusions with salinities between 7 and 11 wt. % NaCl equ., homogenizing between 150 °C to 230 °C. Stratabound/siderite–polysulphide–barite–quartz vein type mineralisation was derived from solutions with salinities between 5 and 19 wt. % NaCl equ., homogenizing between 60 °C and 160 °C, while late stage galena–barite veins were precipitated from solutions with salinities between 11 and 16 wt. % NaCl equ., homogenizing between 100 °C to 140 °C. Fluid inclusion bulk leachate chemistry recorded Na⁺>Mg²⁺>K⁺>Ca²⁺>Li⁺ and Cl⁻>SO₄²⁻ ions. Sulphur isotope composition of barites and overlying gypsum stems from Permian seawater sulphate, supported by increased Br⁻ content, which follows successively the seawater evaporation line. The sulphur isotopic composition of sulphides varies between –0.2 and +12.5 ‰, as a result of thermal reduction of Permian marine sulphate. Ore–forming fluids were produced by hydrothermal convective cells (reflux brine model), and were derived primarily from Permian seawater, modified by evaporation and interaction with Permian sedimentary rocks. Rude deposits in Samoborska Gora Mts. may be declared as a prototype of the Permian siderite–polysulphide–barite deposits (products of rifting along the passive Gondwana margin), in the Inner Dinarides, and their equivalents extending northeastward into the Zagorje–Mid–Transdanubian Zone and the Gemerides, and southeastward to the Hellenide–Albanides.

Keywords: Rude siderite–polysulphide–barite–haematite deposit, Early intracontinental rifting, SEDEX, Feeder zone, Evaporites, Shock quartz, Planar deformation feature, PDFs, Zagorje–Mid–Transdanubian zone, Internal Dinarides

1. INTRODUCTION

The study focuses on the genesis of siderite–polysulphide–barite–haematite mineralisation of Rude, Samoborska Gora Mts., supported by geological observation, fluid chemistry, and isotope composition of sulphides and sulphates. Siderite–polysulphide–barite–quartz deposits (SPBQ) of the Samoborska Gora, Trgovska Gora, and Petrova Gora Mts. are remarkably comparable in geology, mineralogy, geochemistry of fluids and nature of metal sources. SPBQ deposits can be well correlated with similar SPBQ deposits hosted within non–metamorphosed units of the Internal Dinarides. These include Ljubija (NW Bosnia), those in the Zagorje–Mid–Transdanubian zone, Rudabanya (northernmost Hungary, Lower Triassic), siderite–magnesite deposits in the Gemerides (Rudnyani, Nižna Slana, Jelšava and others), and siderite deposits in the Eastern Alps (PROCHASKA & HENJESKUNST, 2007; RADVANEĆ et al., 2004; PALINKAŠ et al., 2008; STRMIĆ PALINKAŠ et al., 2009). The SPBQ deposits of the Samoborska Gora, Trgovska Gora and Petrova Gora Mts. were described by JURKOVIĆ (1958, 1959, 1960, 1961, 1962); JURKOVIĆ & DURN (1988) and ŠINKOVEC (1971). The deposits have a variable appearance, epigenetic veins, stratabound and stratiform characteristics. Replacement ore is present where the Carboniferous carbonates are the host rocks (Trgovska Gora Mts. and Ljubija deposit). According to PALINKAŠ (1985, 1988, 1990); PALINKAŠ et al. (2003, 2008); BOROJEVIĆ ŠOŠTARIĆ (2004); BOROJEVIĆ ŠOŠTARIĆ et al. (2009), these deposits were formed by sub–terrestrial hydrothermal convective cells (*sensu* HARDIE, 1990), or the reflux brine model (*sensu* LEACH et al., 2005), along the passive continental margin, during the Permian Early intracontinental rifting. Sulphur isotopes point to the dominant contribution of the Permian evaporitic sea water, as an ore–forming fluid, modified by interaction with the host rocks. It rules out a Carboniferous distal volcano–exhalative genetical model (JURKOVIĆ, 1988), and linkage with the Alpine type stratabound epigenetic Pb–Zn sulphide deposits, (e.g. Mežica–Bleiberg types in the Alps), as argued for by lead isotopes (KÖPPEL, 1983; PALINKAŠ, 1985). They also differ remarkably in sulphate isotope composition from the Middle Triassic Dinaridic deposits, as do their prominent representatives at Vareš (SEDEX) and Idrija (epigenetic hydrothermal and SEDEX), (PALINKAŠ, 1985, 1988, 1990; PALINKAŠ et al., 2003, 2008).

2. GEOLOGICAL SETTING

The Samoborska Gora and Medvednica Mts. represents the westernmost part of the Zagorje Mid–Transdanubian zone (ZMTZ), (*sensu* PAMIĆ & TOMLJENOVIĆ, 1998; TOMLJENOVIĆ, 2002) or the Sava Composite unit (*sensu* HAAS et al., 2000; Figs. 1A, B). Units in the ZMTZ show Alpine and Dinaridic characteristics, including elements of both the External and Internal Dinarides. The ZMTZ is flanked between two prominent fault zones, the Periadriatic–Balaton and the Zagreb–Zemplin lineament systems. The mountains are composed of Palaeozoic, Mesozoic–Palaeogene and Neogene formations. Tectonostratigraphic units of the Medved-

nica Mts. can be grouped into four main units. Autochthon: 1) Tectonized ophiolite mélange, including all lithological members, from sediments, to basic and ultrabasic igneous components, 2) Palaeozoic–Triassic magmatic–sedimentary complex overprinted by Early Cretaceous metamorphism, 3) Late Cretaceous–Palaeocene flysch, and Allochthon: 4) Triassic and younger sequences belonging mainly to carbonate platform facies (ŠIKIĆ et al., 1978; 1979; BASCH, 1981; ŠIKIĆ, 1995).

The Autochthon of Samoborska Gora Mts. consists only of: 1) Palaeozoic unit, composed of Late Carboniferous dark gray schists, shales and sandstones. Shallowing of the sedimentary basin evolved into a dry–land phase, followed by deposition of fine to coarse–grained sandstones, interlayered with conglomerates, dolostones and evaporites (HERAK, 1956). These deposits are unconformably overlain by an Early Triassic clastic–carbonate unit, followed by Middle and Late Triassic carbonate–marl sediments, with occasional appearances of cherts; 2) Cretaceous mélange is predominantly composed of basalts and diabases within shales, graywackes, conglomerates, radiolarites and limestones of different Mesozoic ages, covered by Neogene sediments. The volcanics, often as basalt–spilite pillow lavas, might be products of a Triassic rifting stage, and Allochthon: 3) is represented by Mesozoic carbonate platform lithotypes.

The basic difference in geology of the Samoborska Gora Mts. in relation to Medvednica Mts. geology is the absence of the Palaeozoic–Triassic magmatic–sedimentary complex overprinted by Early Cretaceous metamorphism in the former, and the presence of ultrabasic members in the ophiolitic mélange of the latter (ŠIKIĆ et al., 1979; TOMLJENOVIĆ, 2000). The common feature is the presence of siderite–polysulphide–barite–quartz deposits, at Rude (Samoborska Gora Mts.) and Bistra (Medvednica Mts.) within the Permian non–metamorphosed clastics. The deposits are confined to Early intracontinental rifting in the northwestern sector of Neotethys and were emplaced along the passive continental margin of Gondwana (PALINKAŠ, 1990; PALINKAŠ et al., 2008).

3. MINERALISATION

The Rude siderite–polysulphide–barite–haematite ore deposit is located within the valley of Gradna creek, in the village of Rude, 25 km west of Zagreb. The mineralisation is hosted by Permian siliciclastic sediments, overlain by gypsum and anhydrite deposits (Fig. 2), and consists of three epithermal ore types (low to intermediate temperature): 1) siderite–polysulphide–barite–quartz veins (Fig. 3A), 2) stratabound siderite–pyrite–barite–quartz ore beds (Fig. 3B), 3) and late stage barite–galena–quartz veins (Fig. 3C), and two stratiform ore types, 4) stratiform haematite–barite–quartz beds (Fig. 3D), and 5) gypsum and anhydrite layers (Fig. 3E).

1) Siderite–polysulphide–barite–quartz veins are below the stratabound siderite–barite–quartz ore bodies on the eastern side of the Gradna valley (Fig. 2) The sulphide veins cut the Palaeozoic sandstones (Fig. 3A). The veins are most

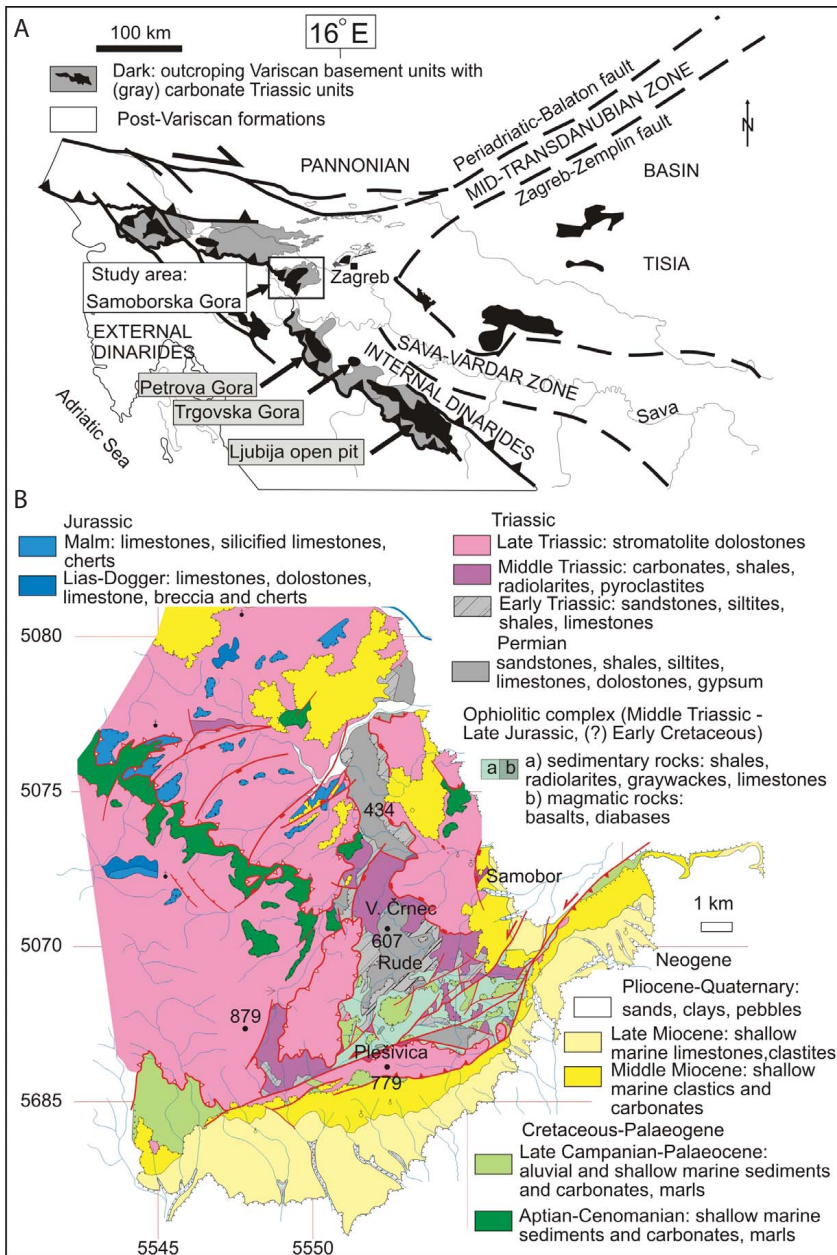


Figure 1: Overview of the major tectonic units of the Zagorje Mid-Transdanubian zone, with geological sketch map of Samoborska Gora Mts. and the location of the Rude mineralisation (PAMIĆ & TOMLJENOVIC, 1998; TOMLJENOVIC, 2002).

commonly cms to dms in thickness, but they can reach up to 3 m in some places (ŠINKOVEC, 1971). Veins predate, are contemporaneous with, and postdate formation of the stratiform–stratabound mineralisation. The vertical extent of the vein–type mineralisation is not more than 40 to 50 m.

Quartz and pyrite, are severely fractured, crushed and brecciated in the veins. However, aggregates of marcasite, pyrite and chalcopyrite, in contrast, show little ductile deformation, due to compensation of the strain by the softer parts of the parageneses. The major vein mineral is siderite, which precipitated earlier than quartz, sulphides and barite.

2) The stratabound siderite–pyrite–barite–quartz ore consists of an iron ore layer extending more than 1.5 km in the NE–SW direction. The central part of the deposit is composed of a yellow–brownish siderite ore body, 180 m long, 80 m wide and up to 8 m thick (average 3–4 m) which dips 25–35° toward the NW (Fig. 2; ŠINKOVEC, 1971).

In the Kokel and Sv. Trojstvo corridors, a massive siderite bed together with ferruginous sandstones, represents the stratabound ore, formed by infiltration of hydrothermal solutions through the footwall sandstones, and partly through the overlying evaporite beds (Figs. 2 and 4). Mineralisation consists predominantly of coarse–grained siderite and quartz aggregates, and minor pyrite, mica and rutile. Siderite mineralisation is underlain by iron–rich sandstones intercalated with 5–20 cm thick layers of clays, marl clays, cherts and siderite. The upper part of the siderite body is represented by iron rich and iron poor gray sandstones with clay intercalations. Quartz pervasively replaces siderite in these ores (Fig. 3B). Widespread silicification, and irregular veining, and in places the anastomosing appearance of quartz aggregates, suggests a hydrothermal origin, as evidenced by fluid inclusion studies (presented in the forthcoming paragraph) rather than diagenetic recrystallization of silica.

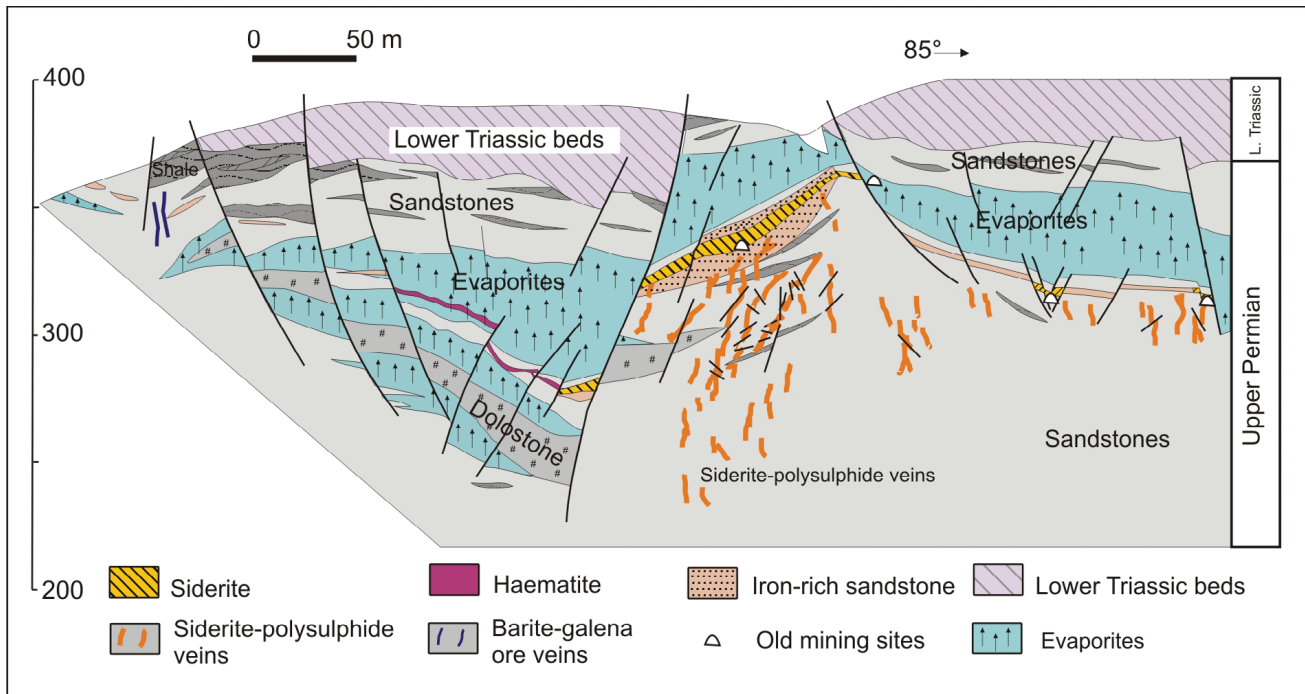


Figure 2: Simplified cross-section through the Rude ore deposit. The principle ore types are: siderite–polysulphide (Cu, Pb, Zn)–barite–quartz veins (designated on the figure as Cu–Fe ore veins), stratabound siderite–barite–quartz beds (on the figure as siderite), stratiform haematite–barite beds (on the figure haematite), and gypsum and anhydrite beds (on the figure as evaporites). Old mining corridors were drawn as trapezoidal openings. The cross-section is in realistic scale based on the mining maps (ŠINKOVEC, 1971).

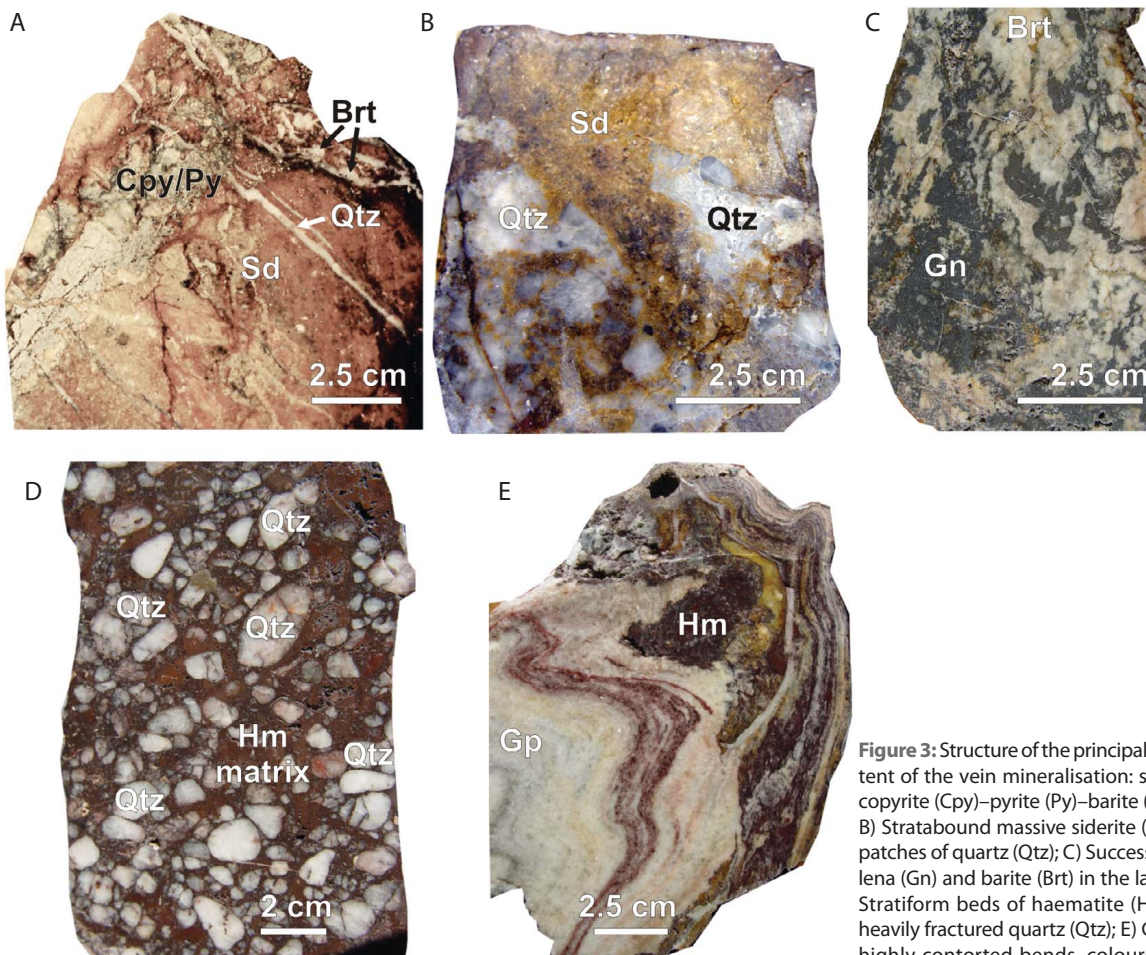


Figure 3: Structure of the principal ore types: A) Content of the vein mineralisation: siderite (Sd)–chalcocopyrite (Cpy)–pyrite (Py)–barite (Brt)–quartz (Qtz); B) Stratabound massive siderite (Sd) with irregular patches of quartz (Qtz); C) Successive growth of galena (Gn) and barite (Brt) in the late stage veins; D) Stratiform beds of haematite (Hm) with detrital, heavily fractured quartz (Qtz); E) Gypsum (Gp) with highly contorted bends, coloured with iron and manganese oxy-hydroxides (Hm).

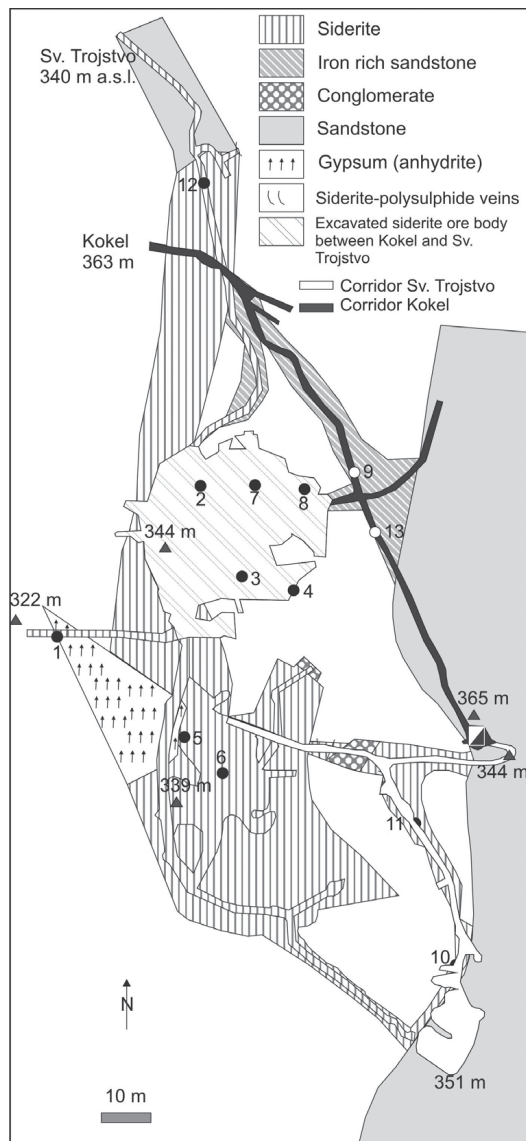


Figure 4: Sketch map of the Sv. Trojstvo and Kokel pits with old mining works (ŠINKOVEC, Mining report, 1954). The numbers and spots mark the sites examined by microscopy.

Stratabound siderite–barite–polysulphide ore, below a gypsum layer, consists of massive yellow–brownish siderite, with pyrite, intensively silicified and partly oxidized (sites, 1., 2., 3., 4., 5., 7.). The reducing conditions during precipitation gradually changed to more oxidizing, evidenced by the presence of barite (sites, 6., 10., 11. and 12.). Stratabound ore in the form of ferruginous quartz sandstones, with siderite cement, partly hematized, microbrecciated, is the lateral extension of the siderite layer. Siderite–sulphide veins intersect or cross the siderite layer.

A change to more oxidizing condition can be deciphered by the presence of barite (Fig. 4) at sites 6, 10, 11, and 12. Pyrite is highly cataclased (Fig. 6; site 10). The massive siderite ore layer laterally grades into the ferruginous sandstone. The siderite cement of the sandstone is gradually converted to a haematitic one, by a process synchronous with mineral precipitation. It is evidenced by the intimate intergrowth of quartz grains and haematitic cement, as well as the absence of traces of box-work or any other supergenic texture, even on a microscopic scale (sites 9 and 13). In contrast to simultaneous precipitation, elsewhere, siderite ore underwent oxidation and attained a micro-brecciated struc-

ture. The exposed siderite sandstones are oxidized by supergenic conditions and quartz grains are coated by colloform goethite, forming garlands, with a cockade ore texture, while a box-work texture developed in the oxidized massive siderite (Figs. 18, 19, 20).

3) Late stage, low-intermediate temperature, galena–barite veins consisting predominantly of galena, barite and minor sphalerite and quartz, cut Upper Palaeozoic sandstones. These are the youngest veins in the Rude ore deposit, and thus they overprint earlier types of mineralisation (Fig. 3C). Maximum thickness is 20–30 cm, and the veins usually end in a network of horstail veinlets.

4) The stratiform haematite–barite–quartz ore (Fig. 3D) consists of small lenticular ore bodies, 5 to 30 m in length, and 1 to 4 m thick. Vertically and laterally this kind of ore passes gradually into ferruginous sandstones with 8 to 30 wt. % iron content. The old mining site and outcrops of the haematite–barite–quartz ore are exposed at the Klassenbruch locality, at the upper riverhead of the Gradna stream.

The stratiform haematite–barite–quartz ore has a homogenous structure (Fig. 3D). The major ore mineral is haematite. In places, barite veinlets, no longer than 4 mm, and barite concretions, mm–cm in size, accompany the major mineral. Quartz is ubiquitous, and sometimes rhythmically alternates with haematite. Haematite conglomerates, with rounded and angular quartz clasts, are matrix- and clast-supported (from a micro- to cm- scale). The origin of quartz is ambiguous, either chemogenic or detrital (Figs. 3D, 21, 22). The problem of detrital quartz in the stratiform ore type was questioned and indicated in the original paper of ŠINKOVEC (1971).

Detrital quartz is marked by a mosaic suture along the grain boundaries (Figs. 21, 22). The shape and sharp contours of the grains, attest little or no transport. Quartz agglomerations, show conical organization of grains, resembling shattered cones. The quartz grains are severely fractured, radially or across the grain boundaries. Jigsaw-fit structures are common (Fig. 21). The deformation features, no wider than 0.1–1 μm , cut across the grains as planar or bent lamellae, closely spaced, following crystallographic planes, usually decorated by fluid and/or mineral inclusions as a result of annealing and healing (FRENCH, 1998). Plastic deformations are easily observed in the form of undulatory extinction on rotation of the stage of the polarizing microscope, which follows the same inclusion-bearing tracks visible in plane polarized light (Fig. 22).

They are referred to as possible shock metamorphic phenomena, induced by meteorite impact at the P/T boundary (KIEFFER, 1971; KIEFFER et al., 1976; GRIEVE et al., 1996; FRENCH, 1998).

There are two possibilities for how quartz entered the ore and sedimentary environment of evaporation. One is being washed into the basin from an already impacted paleorelief, or introduced as an instantaneous impact load into the soft, iron rich mud (the future stratiform ore). Filling of fine jigsaw-fit fractures with haematitic cement, suggests the latter mechanism. More detailed elaboration requires further

research efforts, and the Rude deposits may be an interesting object for the international audience regarding P/T boundary phenomena.

5) The gypsum and anhydrite layers, heavily contorted with red–green–gray–white bands are part of the ore series and are present in the hanging wall of the ore body together with dark dolomite, chert and fine and coarse grained siliciclastics (ŠINKOVEC, 1971, Fig. 3E). The sulphur isotope values suggest their Permian age mimicking the secular variation of the standard Permian sea water. A wide scatter of $\delta^{34}\text{S}$ values in some gypsum specimens, however, indicates a significant contribution of an extraneous source of sulphate ions (ŠIFTAR, 1989), as does a high content of lead.

4. MATERIALS AND METHODS OF STUDY

The samples for ore petrography were prepared by a standard procedure. Cut ore samples were embedded into plastic rings 2–4 cm in diameter, greased, ground (using 120, 240, 400, 600, 800, 1200 mesh quartz powders) and polished (using 6, 3, 1 and 1/2 μm diamond and aluminium powders). A Zeiss Axioplan microscope equipped with a digital camera at Etvös Lorand University, Budapest was used to determine ore minerals, paragenetic successions and distinct textures.

Microthermometric measurements were performed on 0.3–0.5 mm thick wafers of quartz on a Leitz–Wetzlar microscope with objectives P25/0.50 for freezing and UM 32/0.30 for heating runs by a Chaixmeca cooling and heating stage, operating between -180 and $+600$ °C. A Linkam THMS 600 stage was mounted on the Olympus BX 51 microscope using 10x and 50x Olympus long–working distance objective lenses for visible light. Two synthetic fluid inclusion standards (SYN FLINC; pure H_2O , mixed $\text{H}_2\text{O}-\text{CO}_2$), were used to calibrate the equipment. The precision of the system was ± 2.0 °C for the homogenisation temperature, and ± 0.2 °C in the temperature range between -60 and $+10$ °C.

Primary fluid inclusions were determined on the base of their petrography, according to procedure described by ROEDER (1984) and SHEPERD et al. (1985).

Fluid inclusions were measured in: i) quartz associated with stratabound siderite–pyrite–barite–quartz mineralisation; ii) detrital quartz associated with stratiform mineralisation; and iii) barite associated with late stage galena–barite vein mineralisation. The salinity was calculated from ice and hydrohalite melting temperatures using the FLUIDS computer program developed by BAKKER (2003), and according to the procedure described by NADEN (1996). Isochores were calculated using the computer program ISOC (BAKKER, 2003), from the equation of state by ZHANG & FRANTZ (1987), and corrected for the volumetric properties of quartz.

The bulk ion compositions of trapped fluids were analysed by ion chromatography at Montanuniversität Leoben by the technique modified after BOTTRELL et al. (1988). A Dionex DX–500 system was used for analyses of halogens. Cations were analyzed in the aliquots of the same solution using standard atomic absorption spectrometry. The bulk crush–leachate analysis was performed on: i) quartz, haematite and barite associated with stratiform mineralisation; ii) quartz and siderite associated with stratabound mineralisation; and iii) barite and galena associated with late stage galena–barite vein mineralisation.

The sulphur isotope compositions of sulphide ($n=9$) and barite ($n=2$) samples were determined at the Institute of Mineralogy and Geochemistry at the University of Lausanne using the Carlo Erba 1108 elemental analyzer (EA), connected to the Thermo Fischer Scientific Thermoquest/Finnigan Mat Delta S IRMS (EA/IRMS). Barite and gypsum samples were collected from i) stratiform mineralisation. Pyrite, chalcopyrite, sphalerite, galena and barite were sampled from ii) siderite–polysulphide–barite–quartz vein mineralisation, and galena and barite from iii) late stage galena–barite vein mineralisation. The isotope values are reported relative to the Vienna–

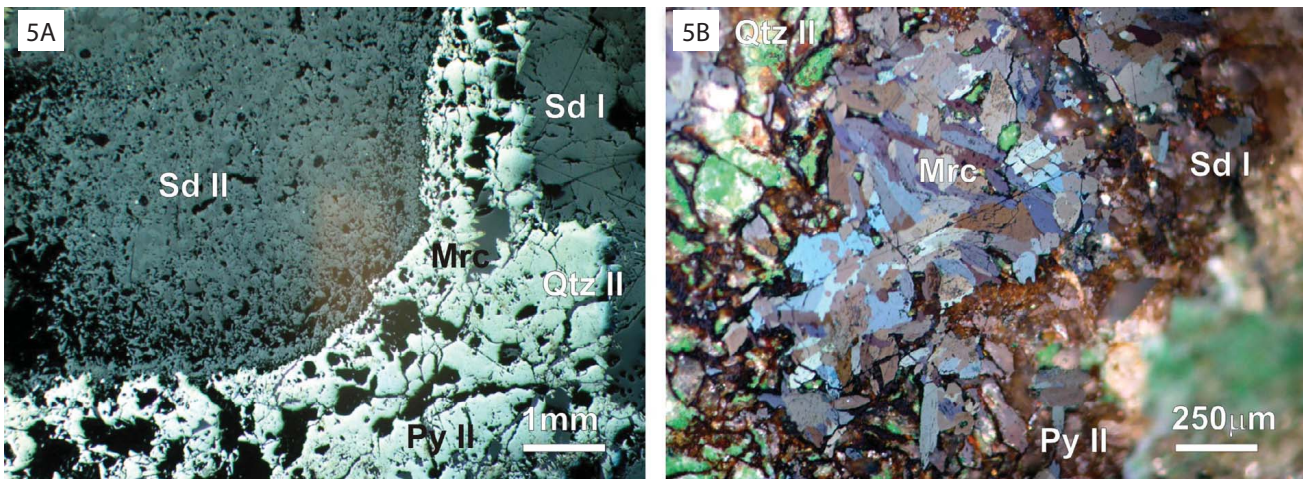


Figure 5: Ore petrography with photomicrographs: A) Coarse grained euhedral siderite I (Sd I), with patches of pyrite II (Py II), accompanied by cogenetic quartz II (Qtz II) and followed by idiomorphic to hypidiomorphic marcasite (Mrc) and fine grained subhedral siderite II (Sd II). Plain polarized light; B) Polars crossed. The photo shows marcasite (Mrc) with expressive anisotropic effects and pyrite II. Because the rate of direct nucleation of FeS_2 is insignificant in slightly acidic solutions below 300 °C, most of the pyrites and marcasites in hydrothermal ores form via the conversion of an FeS precursor. Marcasite can form in excess of 300°C and it can persist on a geological time scale only below 160°C. It has repercussion on the assessment of metamorphic grade of the autochthonous Palaeozoic–Mesozoic formation of Samoborska Gora Mts., which has not been registered yet.

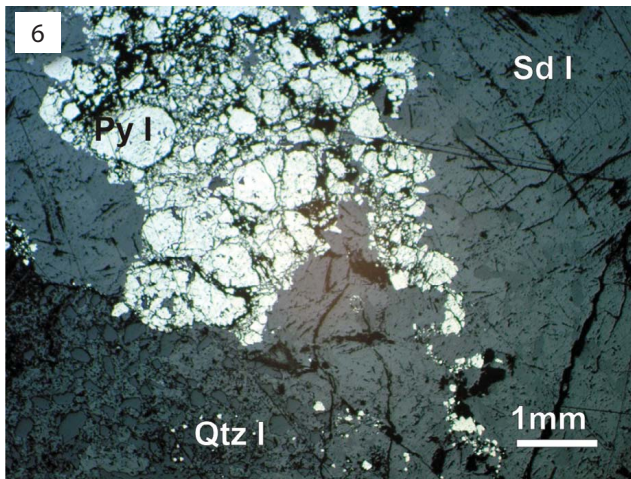


Figure 6: Coarse euhedral grains of siderite I (Sd I), quartz I (Qtz I), and pyrite I (Py I). The pyrite is highly cataclased. Plain polarised light.

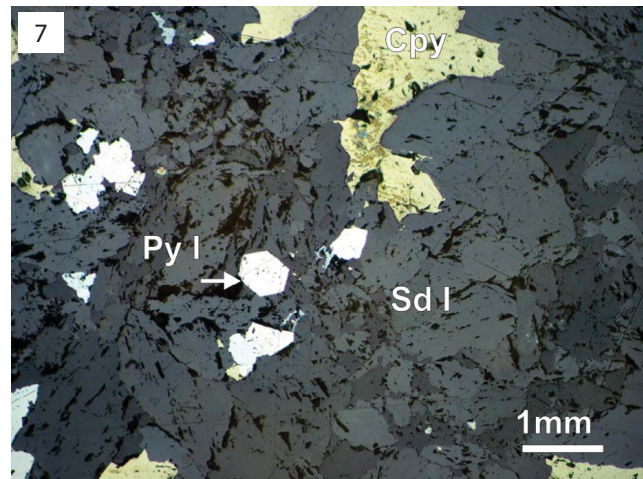


Figure 7: Coarse subhedral grains of siderite I (Sd I), with cogenetic euhedral pyrite I (Py I), and later chalcopyrite (Cpy) within inter-granular space. Plain polarised light.

Canyon Diablo troilite standard (V–CDT). The reproducibility, assessed by replicate analyses of the laboratory standard (pyrite, working value = +6.1 ‰; synthetic mercury sulphide, working value = +15.5 ‰; barium sulphate, working value = +12.5 ‰ $\delta^{34}\text{S}$) was better than 0.2 ‰. Additional sulphur isotope compositions of sulphide (n=4) and barite (n=2) were determined at the National Institute for Research and Development of Isotopic and Molecular Technologies, Cluj–Napoca, Romania.

Major, trace elements and REE in one sample of gypsum from stratiform mineralisation are determined by XRF and ICP-MS at the Bundesanstalt für Geowissenschaften und Rohstoffe in Hannover.

5. PETROGRAPHY

Microscopy of the hydrothermal ore samples from the stratabound and vein type mineralisations determined the following primary minerals: siderite, quartz, pyrite, marcasite, greigite (melnikovite), chalcopyrite, sphalerite, galena, tetrahedrite, linnaeite, barite and chlorite. Secondary minerals are: bornite, chalcocite, covellite, cuprite, and goethite (ŠINKOVEC, 1971).

There are two generations of siderite.

Siderite I (Sd I) is a coarse grained and forms euhedral to subhedral crystals (Figs. 5A, 6, 7), often with annealing effects, with an approximate 120° interfacial angle. Sd I is the major constituent of the vein and stratabound mineralisation, growing simultaneously with quartz I (Qtz I) and pyrite I (Py I) which is often cataclased (Fig. 6).

Siderite II (Sd II) is fine grained, usually euhedral and is associated with marcasite (Mrc) and pyrite II (Py II) (Figs. 5A, B). As the rate of direct nucleation of FeS_2 is insignificant in slightly acidic solutions below 300°C , most of pyrite and marcasite in hydrothermal ores form via conversion of an FeS precursor (SCHOONEN & BARNES, 1991). The pyrite to marcasite ratio from the sulphidation reactions is strongly dependent on pH. Marcasite is the predominant product below pH 5 at 25°C , whereas pyrite is dominant in neu-

tral and alkaline solutions (MUROWCHICK & BARNES, 1986). The same trend is observed at higher temperatures. However, although marcasite can form at temperatures in excess of 300°C , it can only persist on a geological time scale below 160°C (RISING, 1973). It has previously unrecognized repercussions for assessment of the metamorphic grade of the autochthonous Palaeozoic–Mesozoic formation of the Samoborska Gora Mts.

Quartz, beside siderite, is the most abundant mineral in the vein–type mineralisation. There are three generations of quartz:

Quartz I (Qtz I) is cogenetic with siderite I (Fig. 6).

Quartz II (Qtz II) pervasively infills the fractures in siderite I, coprecipitating with pyrite II. (Figs. 3, 9A, B).

Quartz III (Qtz III) is a product of widespread silicification and coexists with all other sulphide minerals and barite (Figs. 11A, B).

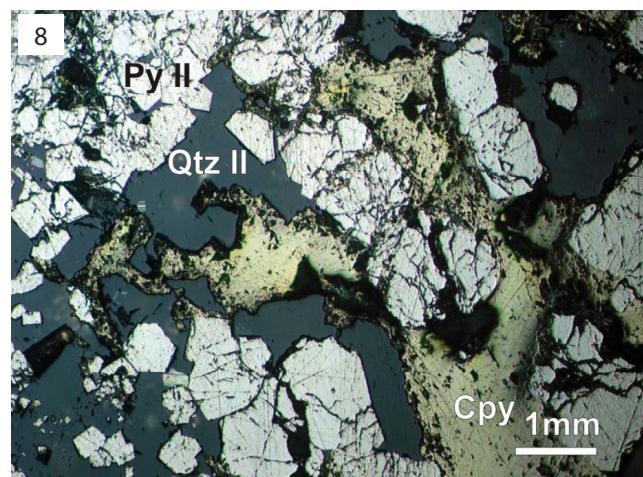


Figure 8: A veinlet of cataclased and idiomorphic pyrite II (Py II), embedded in the quartz II (Qtz II). The silicified siderite host was pervasively penetrated by copper rich solutions. Chalcopyrite (Cpy) resorbed pyrite, producing corroded, granular and rounded interfaces. The pyrite faces, embedded in the quartz stayed perfectly unaffected by advancing replacement. Plain polarised light.

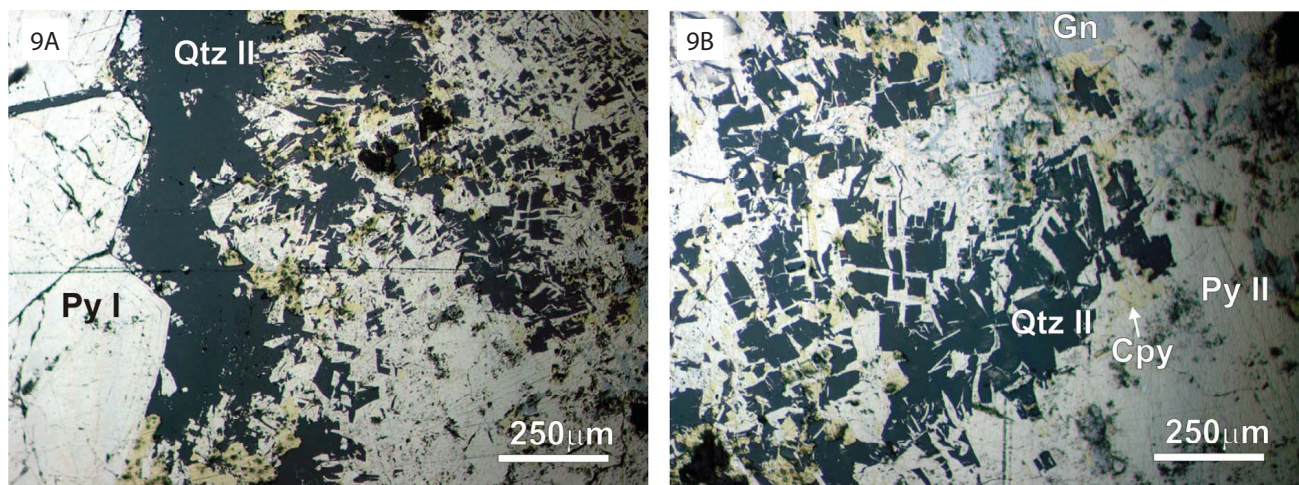


Figure 9: A) Growth zoning; Unobstructed zonal growth of pyrite I (Py I) was gradually retarded by the simultaneous precipitation of quartz II (Qtz II), which converted growth of pyrite into sectorial growth. Plain polarised light; B) The sectorial texture allowed easy penetration of the copper rich solution, through a sieve-like assemblage of quartz and pyrite, and replacement of pyrite grains by chalcopyrite. Replacement of pyrite proceeded by galena (upper right corner). Plain polarised light.

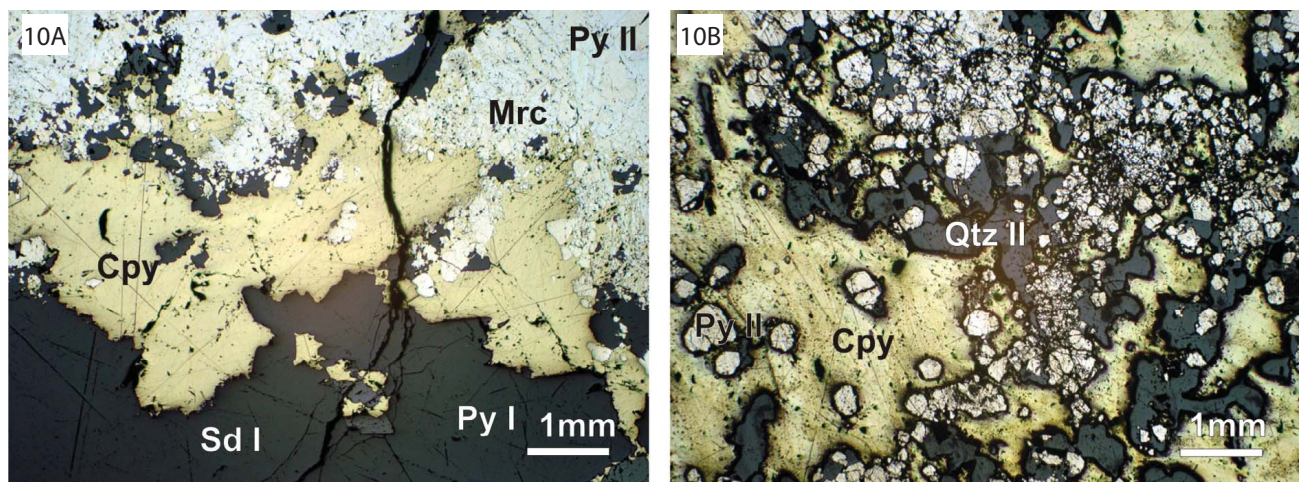


Figure 10: A) Cataclastic pyrite II (Py II), and marcasite (Mrc) minutely disintegrated, and cemented with interstitial quartz II (Qtz II), underwent massive replacement by chalcopyrite (Cpy). Predominantly brittle cataclasis of pyrite and marcasite grains, gradually changed to ductile deformation observed at the right corner of the photo. Plain polarised light; B) Advanced stage of pyrite replacement by chalcopyrite. The quartz II (Qtz II) and pyrite II (Py II) remain as relics of the former veinlet. Pyrite severely cataclasted with crystal faces entirely rounded. Plain polarised light.

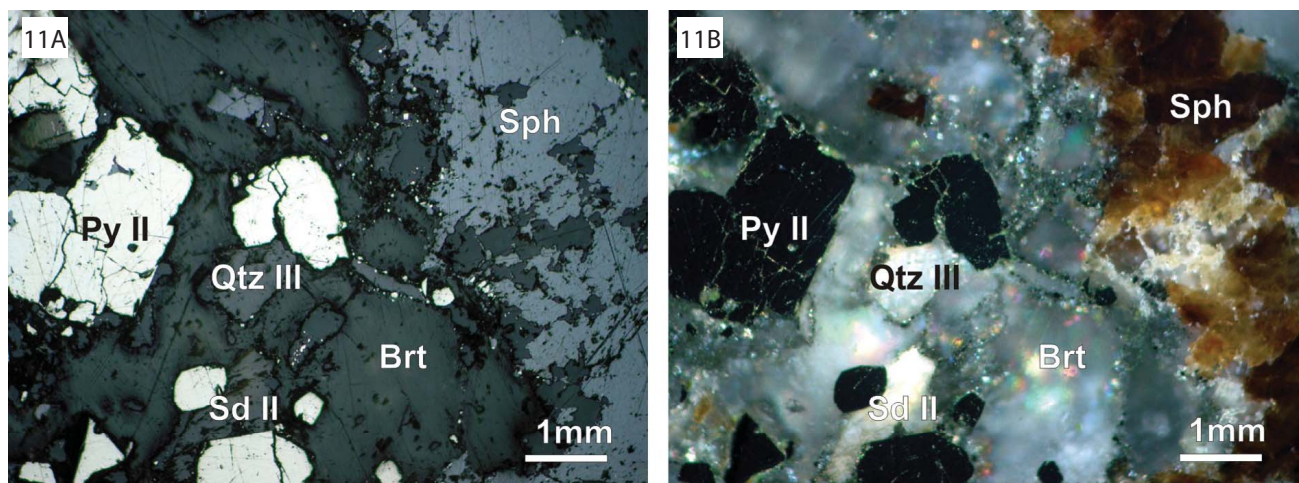


Figure 11: A) Crustification texture. Siderite host crosscut by a symmetrical, crustified veinlet showing successive inward precipitation of minerals, from the open fissure walls: siderite II (Sd II) – quartz III (Qtz III) – pyrite II (Py II) – sphalerite (Sph) – barite (Brt). Central part of the veinlet is filled with barite. Plain polarised light; B) The same microphoto. Crossed polars.

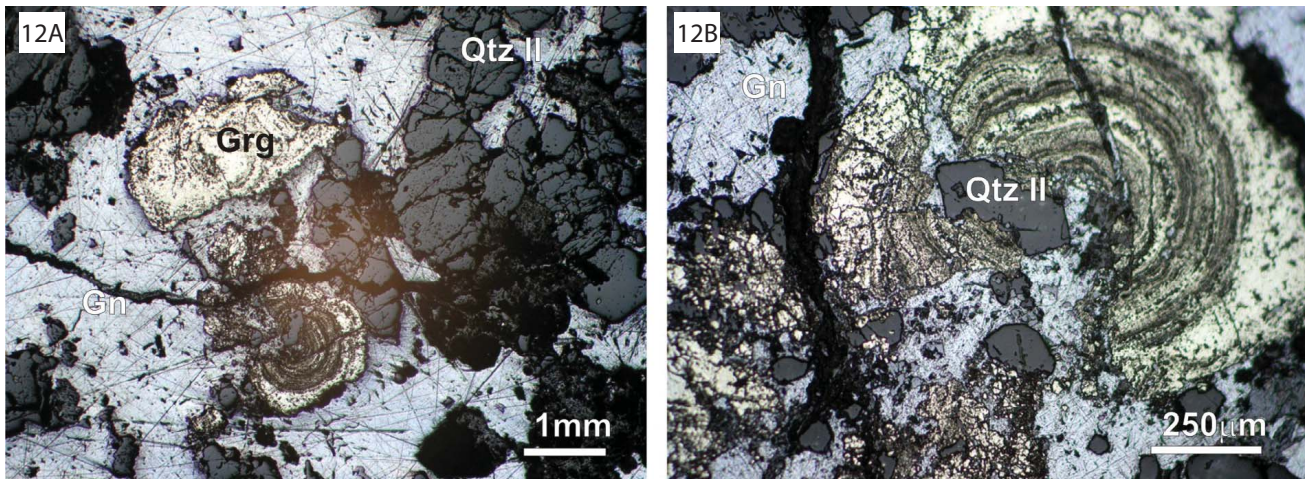


Figure 12: A) Greigite or melnikovite (Grg) forms colloform globular textures, with spheruloids and garlands consisting of radial aggregates. It grows over different nucleation seed cores, usually quartz II (Qtz II). Galena (Gn) post-dates greigite and partly or completely replaces it. Plain polarised light; B) Detailed image of the greigite globular texture. The zonal texture consists of bends, with random, radial or crustified arrangement of aggregate elements. In the center is a quartz grain, serving as a nucleation site. The greigite probably developed over a FeS precursor, gradually converting to pyrite at the outer rims of the globule. The globule is dissected by a galena veinlet, with clear sign of resorption of iron sulphide, and partially infilled by galena. Plain polarised light.

Marcasite; a fine grained aggregates of marcasite usually follows pyrite II, and mark a slight change in the pH of the hydrothermal fluid (Figs. 5A, B).

Greigite (melnikovite) forms colloform spherulites, in places with garland texture (Figs. 12A, B) and represents a late stage phase, however, predating galena and barite. Below 300°C pyrite and marcasite form via an FeS precursor (SCHOONEN & BARNES, 1991).

Chalcopyrite (Cpy) rarely develops idiomorphically, but regularly replaces pyrite and marcasite or just infills the fractured grains (Figs. 7, 10, 13).

Sphalerite (Sph) is rare and is associated with barite (Brt) and galena (Gn) (Figs. 11A, B).

Tetrahedrite (Tet) post-dates and replaces pyrite, likewise chalcopyrite. It occurs before galena but has not been observed as having been replaced by it (Fig. 14).

Galena (Gn) is the youngest member of the paragenesis. It replaces pyrite and chalcopyrite efficiently (Figs. 12A, 13, 15), or infills intergranular spaces in the siderite–quartz host, forming a disseminated style of mineralisation (Figs. 16, 17).

Linnaeite (Ln) is mostly euhedral, regularly embedded in chalcopyrite or occurs as individual grains (Fig. 16).

Barite (Brt) is the youngest mineral phase in the veins, infilling inter-granular spaces induced by fractures (Figs. 11A, B). In the area of Klassenbruch, at the end of the Gradna valley, it forms 10 to 20 cm thick barite–galena (±pyrite, quartz) veins cutting the host sandstones.

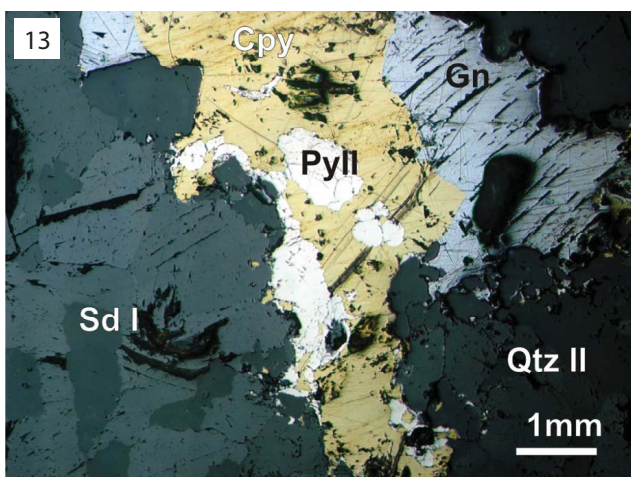


Figure 13: The host, coarse grained siderite (Sd I), experienced several successive replacement events: first silicification and pyritization (Qtz II, Py II), then copper metasomatism, and resorption of pyrite grains, while the galena (Gn) stage is the last one. The cleavage pits in galena are post-depositional features. Plain polarised light.

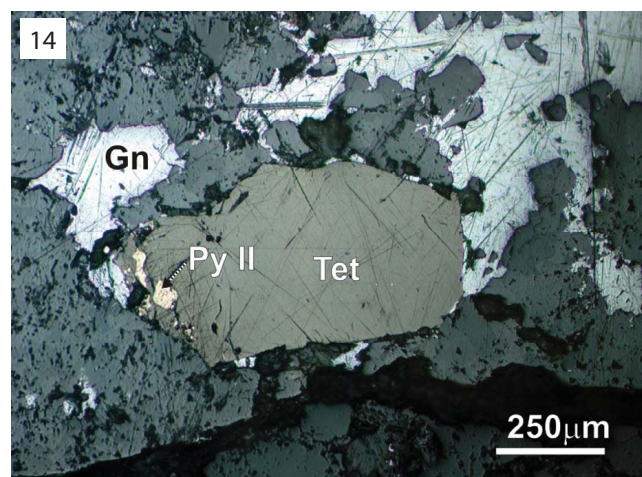


Figure 14: A hypidiomorphic grain of tetrahedrite (Tet) resorbed a pyrite (Py II) grain. The next precipitating phase was galena which penetrated the siderite host, but did not affect the trahedrite grain boundary. Plain polarised light.

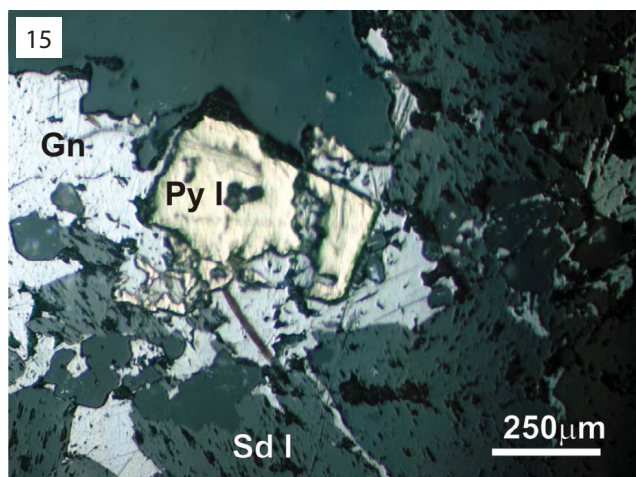


Figure 15: Atoll texture; Resorption of euhedral pyrite by galena in quartz veinlet. The host is siderite I (Sd I). At the bottom of the atoll–Pyrite a tiny grain of pyrite is almost completely replaced. Plain polarised light.

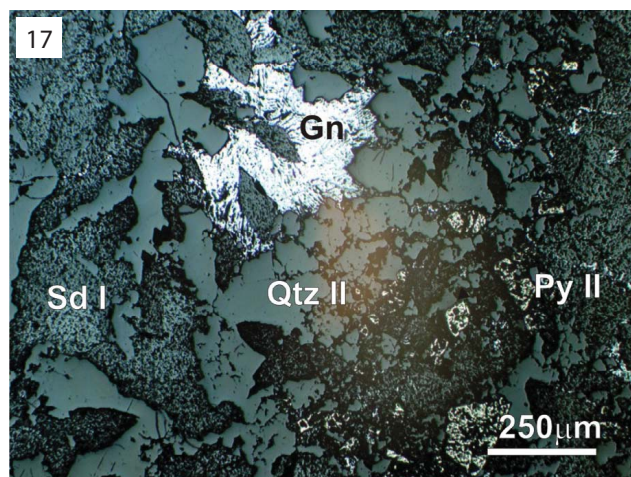


Figure 17: Siderite I (Sd I) host experienced pervasive silicification and pyritization (Py II). Galena (Gn) precipitated next, infilling inter-granular spaces and producing disseminated galena mineralisation. Curved cleavage pits have developed as a result of post-precipitation deformation. Galena replaces all former sulphides. Pyrite II highly corroded. Plain polarised light.

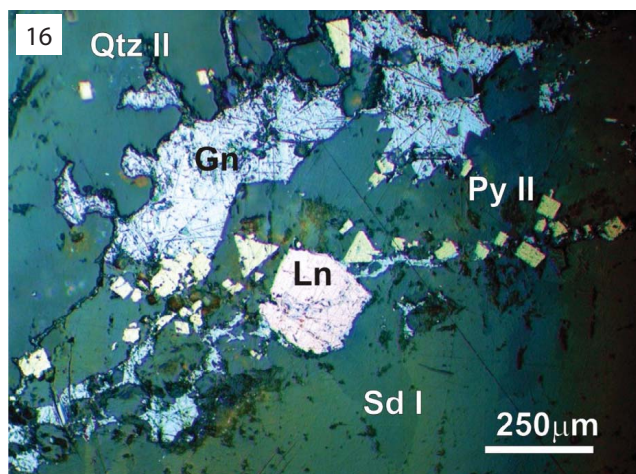


Figure 16: Corona texture; Idiomorphic crystals of pyrite (Py II) and linnaeite (Ln) in the quartz (Qtz II) veinlet, are hosted between walls of coarse crystalline siderite I (Sd I). At the bottom of the large galena grain (Gn) a linnaeite grain (Ln) is replaced by a shapeless aggregate. An idiomorphic crystal of linnaeite, however, persisted to keep a euhedral shape, but a rejuvenated galena veinlet, cut the linnaeite grain diagonally along the former veinlet path, and embraced the linnaeite crystal, forming a corona-like galena rim. Plain polarised light.

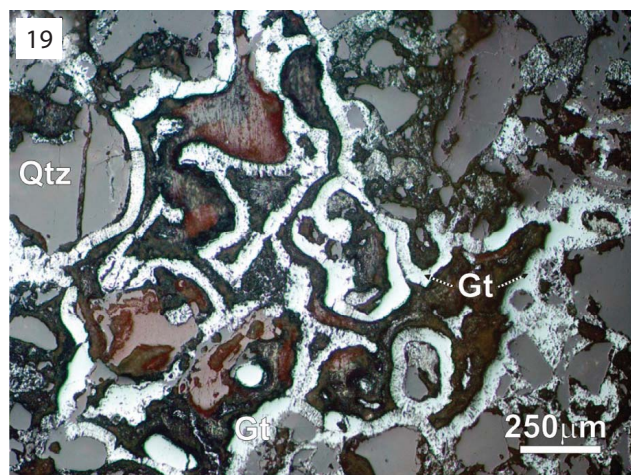


Figure 18, 19: Ferruginous sandstone with siderite cement, oxidized to goethite (Gt), which forms colloform rims around quartz grains (Qtz) in the form of garlands making cockade textures. Plain polarised light.

6. RESULTS

6.1. Fluid inclusion study

1) Quartz associated with stratabound mineralisation contains the following fluid inclusion types with different degree of filling (PALINKAŠ et al., 2003; BOROJEVIĆ ŠOŠTARIĆ, 2004):

- i) primary, liquid-rich inclusions, occasionally containing anisotropic daughter mineral, predominates greatly ($L+V\pm S_A$),
- ii) pseudosecondary, metastable, liquid rich inclusions, sometimes with anisotropic daughter mineral ($L\pm V\pm S_A$). Since the vapor bubble develops after cooling runs, the meta-stability might be induced by ice extension.
- iii) rare vapor rich inclusions ($V+L\pm S_A$), (Figs. 23E, F).

Inclusions are spherical and irregular in shape, and range in size between 5 and 20 μm . During freezing, the following melting sequence was observed (in the presence of a vapour

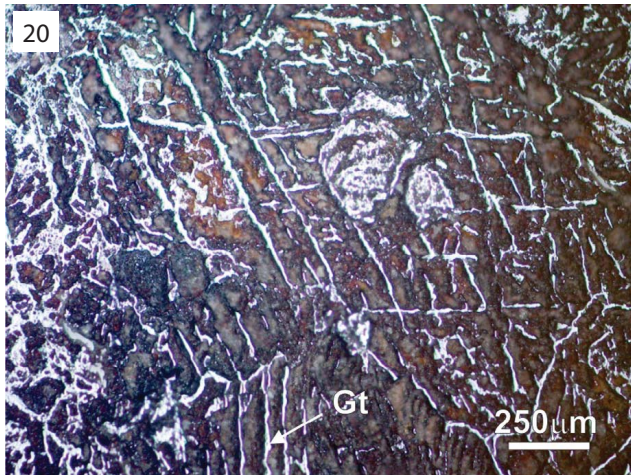


Figure 20: Box-work texture of goethite (Gt) developed after oxidation of massive siderite cement. Plain polarised light.

phase), $I + Hy + A \rightarrow I + Hy + A + Le \rightarrow I + Hy + L \rightarrow I + L \rightarrow L$, where I = Ice, Hy = hydrohalite, A = antarcticite, Le = eutectic liquid and L = Liquid.

First melting (T_c) in a predominant number of liquid–vapour inclusions was observed between $-65\text{ }^\circ\text{C}$ and $-45\text{ }^\circ\text{C}$, indicating the presence of divalent cations in inclusion liquids (Ca^{2+} , Mg^{2+} ; CRAWFORD, 1981; DAVIS et al., 1990). Hydrohalite melting ($T_{m\text{hyd}}$), was observed at temperatures between $-50.0\text{ }^\circ\text{C}$ to $-23.5\text{ }^\circ\text{C}$. Ice melting temperatures ($T_{m\text{ice}}$) are from $-15.5\text{ }^\circ\text{C}$ to $-3.2\text{ }^\circ\text{C}$. Homogenisation to a liquid phase (T_h) occurred at temperatures between $56\text{ }^\circ\text{C}$ and $158\text{ }^\circ\text{C}$. Higher homogenisation temperatures, between $263\text{ }^\circ\text{C}$ and $286\text{ }^\circ\text{C}$, were observed only in two inclusions

Bulk composition was calculated by the melting temperature of ice and hydrohalite. Salinity of fluid inclusions varies between 0.3 to 7.5 mass % NaCl + 4.3 to 14.5 mass % CaCl_2 , with a mass ratio of $\text{NaCl}/(\text{NaCl}+\text{CaCl}_2)$ ranging from 0.07 to 0.76, and the total salinity ranges from 5.3 to 19.2 wt. % NaCl equ.

Several vapour rich inclusions showed high salinity (17.9 to 18.9 wt. % NaCl equ.) and very high homogenisation temperatures (between $352\text{ }^\circ\text{C}$ to $449\text{ }^\circ\text{C}$) to the vapour state (Figs. 24A, C, D). The inclusion behaviour is interpreted as a result of leakage.

2) The following fluid inclusion types were found in barite associated with late stage galena–barite vein mineralisation:

- i) primary, metastable liquid rich inclusions ($L\pm V$),
- ii) pseudo-secondary liquid inclusions (L).

Inclusions with very small sizes ($1\text{--}3\text{ }\mu\text{m}$), occurring in clusters within healed fractures, are interpreted as pseudo-secondary (ROEDDER, 1984, Figs. 23G, H, I). The last melting of ice was registered at temperatures from $-12.2\text{ }^\circ\text{C}$ to $-7.8\text{ }^\circ\text{C}$. The homogenisation to liquid occurs at temperatures between $102\text{ }^\circ\text{C}$ and $140\text{ }^\circ\text{C}$. The total salinity of fluid inclusions was estimated to be between 11.5 and 16.2 wt. % NaCl equ. (Table 1, Figs. 24B, C).

3) Fluid inclusions in detrital quartz associated with stratiform type of mineralisation

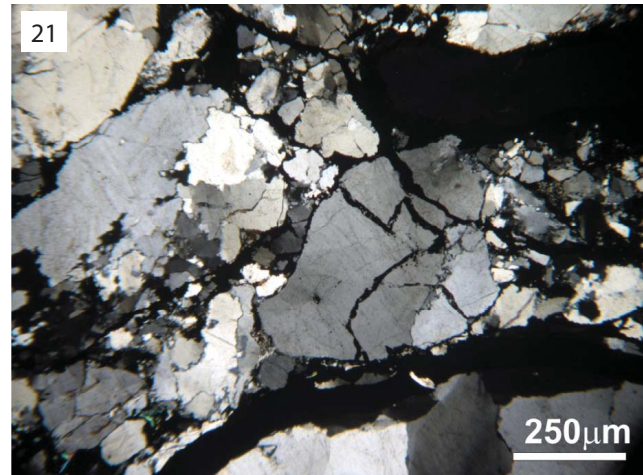


Figure 21: Detrital quartz in the stratiform haematite beds, has developed mosaic suture joints. Planar deformation features (PDFs) cross the grain boundaries. Jigsaw-fit feature on the central grain postdate the PDFs. Plain polarised light.

Detrital quartz intergrown with haematite was separated from haematite–barite–quartz samples (Fig. 3 d) from the sedimentary part of the Rude deposit and the following types of fluid inclusion were observed in them:

- i) secondary, metastable liquid rich inclusions ($L\pm V$),
- ii) secondary liquid inclusion (L), (Figs. 21, 22, 23A, B, C, D).

Microthermometric measurements were performed only on inclusions that nucleated vapour bubble after cooling runs. Due to the very small size of the inclusions ($1\text{--}4\text{ }\mu\text{m}$), during cryometric measurements, only the last melting of ice ($T_{m\text{ice}}$) was registered at temperatures from $-7.5\text{ }^\circ\text{C}$ to $-1.1\text{ }^\circ\text{C}$ (Table 1). The homogenisation to liquid (T_h) occurred at temperatures between 150 and $231\text{ }^\circ\text{C}$. The total salinity of fluid inclusions is between 7.2 and 11.1 wt. % NaCl equ. (Table 1; Figs. 24B, C).

High temperature of homogenisation (T_h), with salinities between 7.2 and 11.1 wt. % NaCl equ. would suggest an

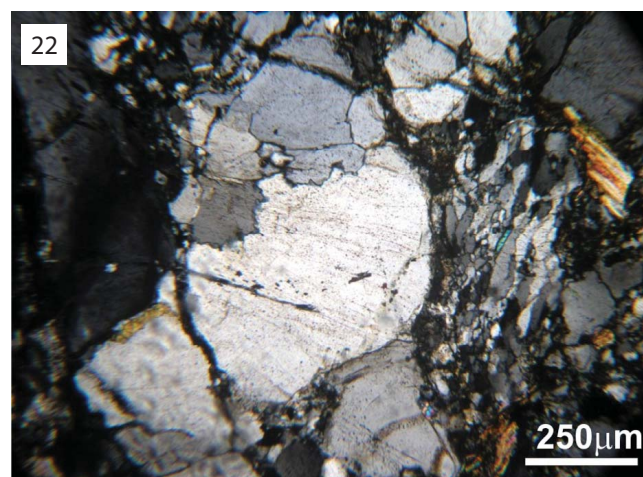


Figure 22: PDFs in detrital quartz are decorated by solid and fluid inclusions visible under high magnification only.

Table 1: Microthermometric data grouped according to the inclusion types in quartz from stratabound siderite-barite-quartz mineralisation, detrital quartz associated with stratiform mineralisation, and in barite from the late stage galena-barite veins.

Quartz, stratabound/vein type ore											
Fl type	F	T _c (°C)	T _{m hyd} (°C)	T _{m ice} (°C)	T _h (°C)	s (wt.%NaCl equ.)	ρ (g/cm ³)	Molality	wt.% NaCl	wt.% CaCl ₂	NaCl/NaCl+CaCl ₂
L+V	0.95	-65.0	-50.2	-10.1	122.5	14.1	1.040	2.807	1.0	13.8	0.07
L+V	0.90		-40.8	-12.5	115.0	16.5	1.060	3.388	2.0	14.0	0.13
L+V	0.90	-49.0	-44.0	-11.1	112.0	15.1	1.056	3.053	1.5	14.5	0.09
L+V	0.95	-48.8	-45.3	-10.8	132.5	14.8	1.038	2.980	1.3	13.8	0.08
L+V	0.95		-27.4	-7.4	263.5		0.878	2.112	5.5	5.8	0.49
L+V	0.95		-26.8	-9.6	158.0	13.6	1.017	2.682	7.5	6.0	0.56
L+V	0.98			-6.8	132.8	10.2	1.006	1.952			
L+V	0.90			-6.1	286.0		0.833	1.762			
L+V	0.95			-6.1		9.3					
L+V	0.98		-27.0	-6.0		9.2			5.3	4.3	0.55
L+V	0.98		-27.0	-5.7		8.8			5.0	4.3	0.54
L+V	0.98		-27.0	-5.7		8.8			5.0	4.3	0.54
L+V	0.95		-48.0	-6.2	124.0	9.5	1.007	1.789	0.5	9.8	0.05
L+V	0.98			-5.8	114.4	8.9	1.011	1.680			
L+V	0.98			-3.8	109.0	6.1	0.996	1.120			
L+V	0.98			-3.2	137.4	5.3	0.969	0.947			
L+V	0.98				111.8						
L+V	0.98	-45.0	-34.0	-5.0	112.4	7.9	1.005	1.458	2.0	6.8	0.23
L+V	0.95	-62.2	-38.0	-5.7	139.0	8.8	0.991	1.653	1.0	8.8	0.10
L+V	0.95	-61.0	-36.2	-5.2	137.5	8.1	0.998	1.514	1.0	8.0	0.11
L+V	0.95	-60.7	-38.5	-5.2	126.5	8.1	0.997	1.514	0.8	8.8	0.08
L+V	0.98	-62.5	-49.1	-11.2	114.1	15.2	1.054	3.078	0.8	15.0	0.05
L+V	0.95	-62.5	-33.5	-6.9		10.4			2.5	8.0	0.24
L+V	0.98	-58.1	-38.0	-4.4	112.0	7.0	1.000	1.290	0.8	6.3	0.11
L+V	0.98	-57.6	-38.5	-4.4	110.3	7.0	1.001	1.290	0.3	6.3	0.04
L+V	0.95	-66.5		-4.7		7.4					
L+V	0.95	-47.5	-23.5	-6.2		9.5			7.3	2.3	0.76
L+V	0.85	-52.0	-27.1	-6.3		9.6			5.3	4.5	0.54
L+V	0.98	-53.0	-31.3	-13.1	107.4	17.1	1.073	3.528	5.5	4.5	0.55
L+V	0.95	-55.5	-29.6	-15.5		19.2			4.0	14.3	0.22
L+V	0.98		-36.2	-5.2	120.4	8.1	1.000	1.514	1.8	7.3	0.19
L+V	0.98	-58.8	-38.5	-5.2	121.8				0.8	8.8	0.08
L+V	0.95				148.8						
L+V	0.95				122.0						
L+V+S _A	0.98				125.6						
L+V+S _A	0.95	-58.7	-38.5	-4.8		7.6			0.8	7.5	0.09
V+L	0.15	-46.2	-31.5	-14.8		18.6	0.842	3.914	5.8	12.0	0.32
V+L	0.15		-32.0	-14.0		17.9	0.697	3.734	5.3	12.3	0.30
V+L	0.25		-31.5	-15.0		18.8	0.821	3.959	6.0	12.5	0.32
L±V	0.98	-56.0	-33.2	-8.5	78.3	12.3	1.059	2.401	3.5	9.0	0.28
L±V	0.98	-45.0	-34.0	-5.1	97.0	8.0	1.016	1.486	2.0	7.0	0.22
L±V	0.98	-62.2	-36.2	-5.1	56.0	8.0	1.040	1.486	1.8	7.5	0.19
L±V	0.95			-9.7	96.0	13.7					
L±V	0.95			-9.4	94.0	13.3					
L±V	0.98	-51.2	-30.1	-4.5	83.6	7.2	1.019	1.318	2.3	4.0	0.36
L±V	0.98	-54.5	-32.4	-9.2	81.0	13.1	1.064	2.580			
L±V			-28.8	-6.1	97.0	9.4	1.025	1.762			
L±V			-28.8	-5.2	86.0	8.1	1.024	1.514			
L±V		-55.0	-30.6	-5.5	90.0	8.5	1.024	1.597			
L±V		-55.0	-29.8	-5.1	102.0	8.0	1.013	1.486			

Table 1: continued

Quartz, stratiform ore											
FI type	F	T _e (°C)	T _{m,hyd} (°C)	T _{m,ice} (°C)	T _h (°C)	s (wt.%NaCl equ.)	ρ (g/cm ³)	Molality	wt.% NaCl	wt.% CaCl ₂	NaCl/NaCl+CaCl ₂
L±V	0.98				73.0						
L±V	0.95			-7.5	191.0	11.1		2.135			
L±V	0.98				155.0	9.2					
L±V	0.98			-1.1	155.0	9.2	0.959	0.333			
L±V	0.98				150.0	9.2					
L±V	0.98			-6.1		9.3		1.762			
L±V	0.95			-4.5	231.0	7.2	0.890	1.318			
Barite, late Brt–Gn veins											
FI TYPE	F	T _e (°C)	T _{m,hyd} (°C)	T _{m,ice} (°C)	T _h (°C)	s (wt.%NaCl equ.)	ρ (g/cm ³)	Molality	wt.% NaCl	wt.% CaCl ₂	NaCl/NaCl+CaCl ₂
L±V	0.98			-12.2	102.0	16.2	1.059	3.316			
L±V	0.98			-10.3	122.0	14.3	1.029	2.856			
L±V	0.98			-7.8	108.0	11.5	1.018	2.216			
L±V	0.98			-9.0	138.0	12.9	1.008	2.529			
L±V	0.98			-9.0	128.0	12.9	1.015	2.529			
L±V	0.98			-10.0	140.0	14.0	1.015	2.782			
L±V	0.98			-9.0	117.0	12.9	1.022	2.529			

unrealistic pressure of fluids originating in a shallow depositional environment. It suggests another origin of fluid inclusions, as well as their resemblance to PDFs.

6.2. Bulk crush–leach analysis

The bulk crush–leach analysis was undertaken on the fluid inclusions in anticipation that the primary inclusions were the predominant group, as attested to by fluid inclusion (FI), microscopy. Detrital quartz in the stratiform ore, however, contains mostly secondary FIs, following the deformation features, not wider than 0.1–1 μm, cross-cutting the grains as planar or bent lamellae.

1) Samples associated with stratabound/vein sulphide mineralisation

Data obtained in quartz and siderite from the vein type siderite–polysulphide–barite–quartz mineralisation show dominant Na⁺ and Mg²⁺ cations, followed by K⁺ and Ca²⁺. The dominant anion is Cl⁻ (Table 2). The data confirmed the presence of divalent Mg²⁺ and Ca²⁺ cations within fluids, predicted by cryometry. The mass balance shows an excess of cations (Q⁺/Q⁻ from 2.4 to 8.2), similar to the samples from the stratiform part of the deposit.

2) Samples associated with late stage galena–barite veins

Barite and galena were analyzed from the late stage galena–barite vein mineralisation. The dominant cations are Na⁺ and Mg²⁺, while the dominant anion is chlorine within barite, and sulphate within galena. The mass balance (Q⁺/Q⁻) ranges from 0.8 to 1.4 (Na⁺>Mg²⁺>K⁺>Ca²⁺>Li⁺, Table 2). Late stage barite–galena veins were precipitated from moderate salinity–low temperature fluids (salinity between 11.5 and 16.2 wt. % NaCl equ., T_h between 102 °C and 140 °C).

3) Samples associated with stratiform mineralisation

The bulk crush–leach analysis was performed on detrital quartz, haematite and barite associated with the haematite mineralisation. Calculated ion ratios reveal the presence of predominantly Na–Mg–Ca–K chloride solutions. The amount of SO₄²⁻ is increased in haematite samples (ratio Cl⁻/SO₄²⁻, from 0.1 to 0.4). Leachate of the haematite samples confirms a Mg–K–Ca–Na sulphate rich solution. The mass balance (Q⁺/Q⁻) ranges from 1.0 to 7.1. Several samples show an excess of cations (up to 9.6), attributed to a possible high CO₃²⁻ and/or HCO₃⁻ concentration within bulk fluids (due to the onset of siderite precipitation), which were not measured during the procedure (Table 2).

6.3. Sulphur isotopes

1) Siderite–polysulphide–barite–quartz veins

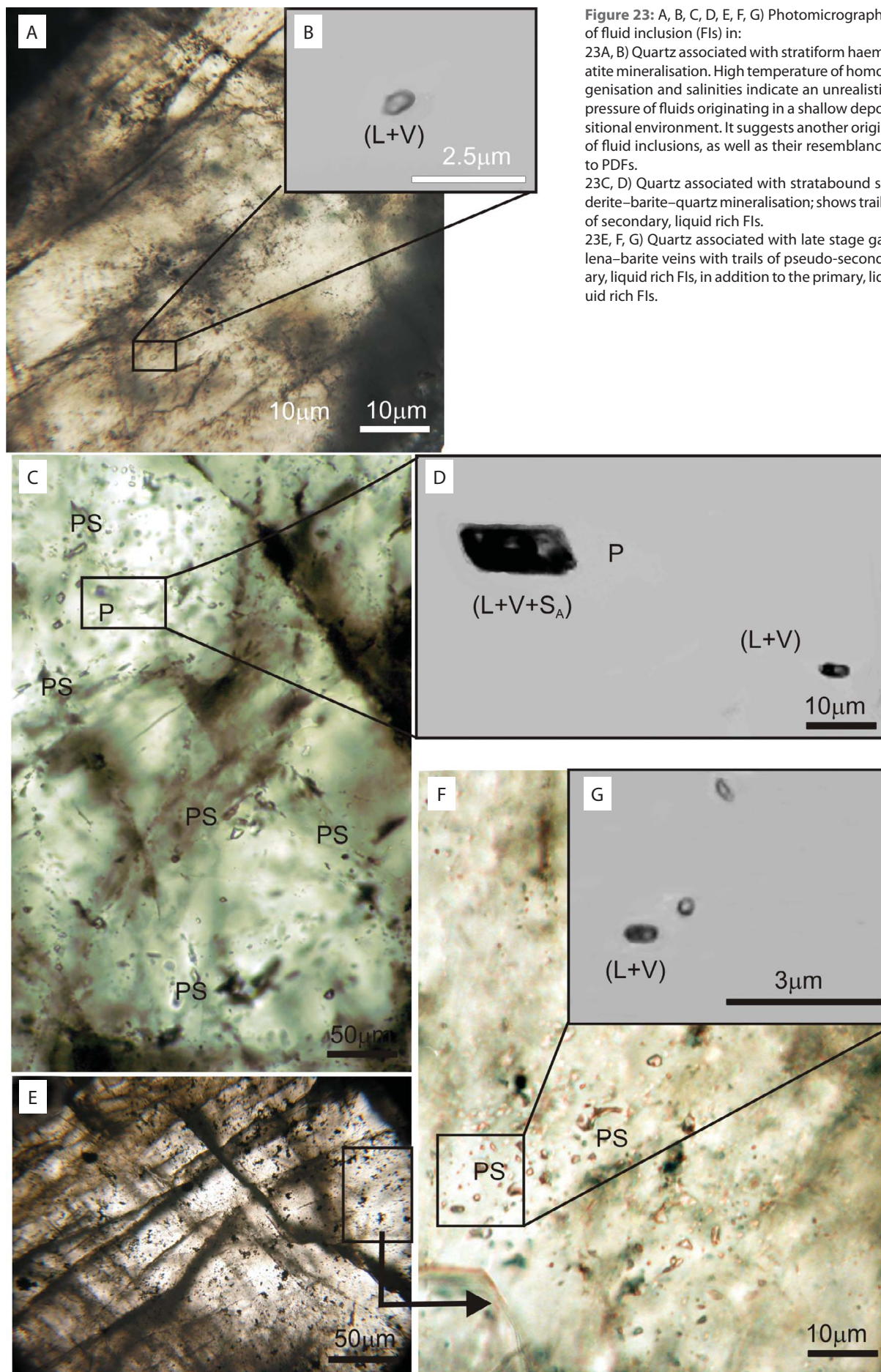
Fifteen sulphide samples from the siderite–polysulphide–barite–quartz veins were analyzed. Their isotopic compositions range between -0.2 and +12.5 ‰ V–CDT. Pyrite varies between -0.2 and +11.1 ‰, chalcopyrite between -0.2 and +1.2 ‰, galena between +1.7 and +7.3 ‰ and sphalerite from +11.3 to +12.5 ‰. Values increased from chalcopyrite towards galena and sphalerite (Fig. 26, Table 3).

2) Stratiform mineralisation

The δ³⁴S values of sulphates (gypsum and barite) in the stratiform mineralisation span between +3.2 and +13.6 ‰ V–CDT (Fig. 26).

3) Late stage galena–barite vein type mineralisation

Two pairs of barite and galena samples were analyzed from the late stage galena–barite vein type mineralisation. Isotopic values vary from +1.7 to +4.6 ‰ for galena and between +5.8 and +8.7 ‰ for barite samples (Fig. 26).



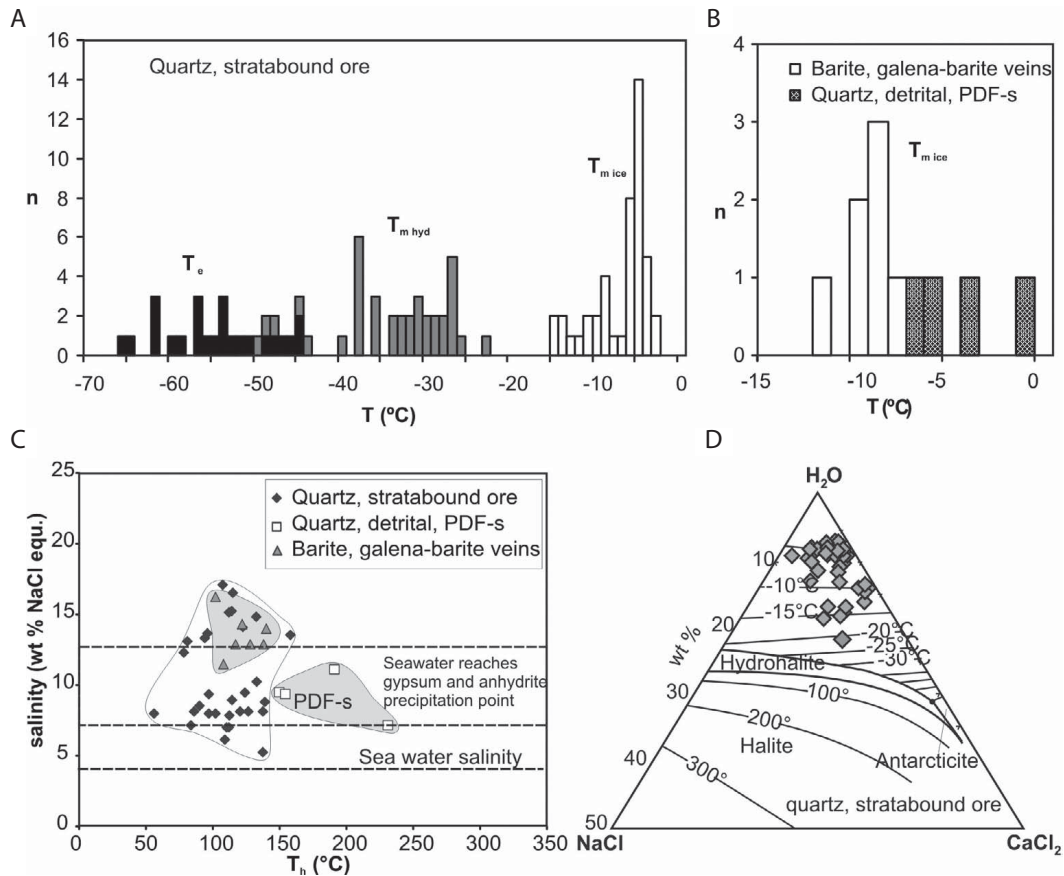


Figure 24: Chemical and microthermometric data of studied fluid inclusions: A) Temperature of eutecticum (T_e), melting of hydrohalite ($T_{m\text{hyd}}$), melting of ice ($T_{m\text{ice}}$) in FIs of quartz from stratabound ore; B) Temperature of melting of ice ($T_{m\text{ice}}$) in quartz from the late stage galena–barite veins, and detrital quartz from the stratiform mineralisation; C) Salinity vs. temperature of homogenisation (T_h) in quartz from stratabound ore, detrital quartz (PDFs) in stratiform mineralisation, and barite in late stage galena–barite veins; D) Three component diagram H_2O – NaCl – CaCl_2 of melting of the last solid phase (ice).

Table 2: Bulk crush–leachate data of siderite, barite, haematite and quartz from stratiform, stratabound and late stage galena–barite veins from Rude.

Sample No.	Mineral	Location	Li^+ ($\mu\text{mol/l}$)	Na^+ ($\mu\text{mol/l}$)	K^+ ($\mu\text{mol/l}$)	Mg^{2+} ($\mu\text{mol/l}$)	Ca^{2+} ($\mu\text{mol/l}$)	Cl^- ($\mu\text{mol/l}$)	I^- ($\mu\text{mol/l}$)	Br^- ($\mu\text{mol/l}$)	SO_4^{2-} ($\mu\text{mol/l}$)	Q^+/Q^-	K^+/Na^+	$(\text{Br}/\text{Cl}) \cdot 1000$	$\text{SO}_4^{2-}/\text{Cl}^-$
S3/B	Quartz	Stratiform ore	0.12	113.92	14.71	96.32	6.72	83.36	1.90	0.30	15.93	2.85	0.13	3.65	0.19
S6/B	Quartz	Stratiform ore	0.18	102.99	14.71	94.09	402.49	88.33	1.68	0.44	12.31	9.66	0.14	5.03	0.14
S5/A	Barite	Stratiform ore	0.29	176.51	14.46	92.08	96.01	169.42	0.68	0.47	177.90	1.08	0.08	2.78	1.05
S7/B	Barite	Stratiform ore	0.33	110.48	11.06	93.07	26.49	111.08	1.97	0.57	55.07	1.61	0.10	5.13	0.50
S6/A	Haematite	Stratiform ore	0.41	44.73	123.81	82.29	1.95	21.11	3.55		71.02	2.02	2.77		3.36
S5/B	Haematite	Stratiform ore	0.91	41.86	71.97	110.43	470.20	26.96	2.87		74.76	7.11	1.72		2.77
S7/A	Haematite	Stratiform ore	0.80	23.36	60.06	99.98	28.45	7.96	2.36		74.62	2.14	2.57		9.38
S3/A	Haematite	Stratiform ore	0.33	51.06	62.95	82.29	24.68	22.32	2.58		52.79	2.52	1.23		2.37
S9/B	Quartz	Stratabound/ vein type ore	0.54	83.46	34.84	91.92	1.95	118.19	1.33	0.39	3.07	2.43	0.42	3.30	0.03
77a	Quartz	Stratabound/ vein type ore	0.24	74.03	24.07	90.63	1.29	82.68	1.71	0.32	6.17	2.91	0.33	3.85	0.07
S9/A	Siderite	Stratabound/ vein type ore	0.37	117.76	16.86	364.84	30.33	112.29	1.79	0.37	21.06	5.91	0.14	3.32	0.19
S10	Siderite	Stratabound/ vein type ore	0.35	113.42	11.17	414.60	145.41	119.86	2.75	0.51	14.06	8.23	0.10	4.29	0.12
S8/B	Barite	Late Ba-Gn veins	0.37	214.88	13.54	91.46	5.46	193.75	1.39	0.49	56.09	1.37	0.06	2.52	0.29
S8/A	Galena	Late Ba-Gn veins	0.47	71.11	18.55	195.11	15.19	40.06	4.33		278.07	0.85	0.26		6.94

Table 3: Sulphur isotope values ($\delta^{34}\text{S}$, ‰) of sulphides and sulphates.

Sample No.	Mineralisation type	Mineral	$\delta^{34}\text{S}$ (‰)	Reference
SG 1	gypsum strata	gypsum	13.4	Šiftar, 1989
SG 2	gypsum strata	gypsum	13.6	Šiftar, 1989
SG 3	gypsum strata	gypsum	13.4	Šiftar, 1989
SG 4	gypsum strata	gypsum	10.8	Šiftar, 1989
SG 5	gypsum strata	gypsum	11.8	Šiftar, 1989
SG 6	gypsum strata	gypsum	10.5	Šiftar, 1989
SG 7	gypsum strata	gypsum	6.7	Šiftar, 1989
SG 8	gypsum strata	gypsum	3.2	Šiftar, 1989
SG 9	gypsum strata	gypsum	7.2	Šiftar, 1989
SG 10	gypsum strata	gypsum	6.2	Šiftar, 1989
SG 11	gypsum strata	gypsum	3.6	Šiftar, 1989
SG 12	gypsum strata	gypsum	8.4	Šiftar, 1989
SG 13	gypsum strata	gypsum	9.6	Šiftar, 1989
SG 18	gypsum strata	gypsum	11.1	This study
SG 14	stratiform (haematite)	gypsum	7.1	Šiftar, 1989
SG 100	stratiform (haematite)	barite	6.0	This study
SG 15	stratabound/vein type*	barite	11.6	Šiftar, 1989
SG 16	stratabound/vein type*	galena	3.0	Šiftar, 1989
SG 104	stratabound/vein type*	galena	7.3	This study
SG 306-1	stratabound/vein type*	pyrite	1.2	This study
SG 304-1	stratabound/vein type*	pyrite	1.1	This study
SG 105	stratabound/vein type*	pyrite	-0.2	This study
SG 301-2	stratabound/vein type*	pyrite	9.9	This study
SG 303-2	stratabound/vein type*	pyrite	11.1	This study
SG 304-2	stratabound/vein type*	chalcopyrite	0.6	This study
SG 306-2	stratabound/vein type*	chalcopyrite	1.2	This study
SG 17	stratabound/vein type*	chalcopyrite	0.6	Šiftar, 1989
SG 103	stratabound/vein type*	chalcopyrite	-0.2	This study
SG 303-1	stratabound/vein type*	sphalerite	12.5	This study
SG 305-1	stratabound/vein type*	sphalerite	11.3	This study
SG 102	late Brt-Gn veins	barite	5.8	This study
SG 302-2	late Brt-Gn veins	barite	8.7	This study
SG101	late Brt-Gn veins	galena	1.7	This study
SG 302-1	late Brt-Gn veins	galena	4.6	This study

* quartz-polymetallic-siderite

6.4. Geochemistry of a selected gypsum sample

Major elements (XRF, %), trace elements (ICP-MS, ppm) and REE (ICP-MS, ppm) of the selected gypsum sample from the stratiform mineralisation are presented in Table 4.

7. DISCUSSION

Fluid inclusion data indicate differences in precipitation conditions for the stratiform and stratabound/vein types of mineralisation (Fig. 24C).

The vein/stratabound mineralisation precipitated from fluids with highly variable salinities (between 5.3 to 19.2 wt. % NaCl equ.), and homogenisation temperatures between 56 °C and 158 °C (Fig. 24C).

Late stage barite–galena veins precipitated from moderate salinity–low temperature fluids (salinity between 11.5 and 16.2 wt. % NaCl equ., and T_h between 102 °C and 140 °C). All measured salinities are increased relative to seawater, and the predominant portion of salinities corresponds to the composition of seawater that passed the gypsum and anhydrite precipitation point (Figs. 24C, 25A, B). At some point, meteoric water entered into the system, causing dilution down to 5.3 wt. % NaCl equ.

The intrusion of meteoric water is a plausible explanation for coexistence between low salinity and a high Br/Cl ratio. Fresh water with low concentrations of Br⁻ and Cl⁻ would have not affected their ratio but would have decreased the salinity. The chemistry of the late stage galena–barite vein changed to become more sodic in comparison to the stratiform ore which shows an expressive calcic character.

The bromine/chlorine concentration ratio in quartz and barite leachates corresponds to 6.5–10.5 % of recent seawater evaporation. Some part of the samples follow a seawater evaporation trend (SET) to a high percentage of seawater evaporation (Figs. 25A, B). The Br/Cl ratios demonstrate clustering of data between 15 and 35 % of seawater evaporation, but the high excursion of K/Na ratios, exceeding 2 to 3 times the evaporitic concentration, is probably due to hydrothermal water/rock interactions (McCAFFREY et al., 1987). Ore forming fluids underwent different degrees of evaporation, whereas a maximum degree of 35 % (according to Br/Cl ratios) indicates that brines locally passed the halite saturation point. These is in disagreement with the ob-

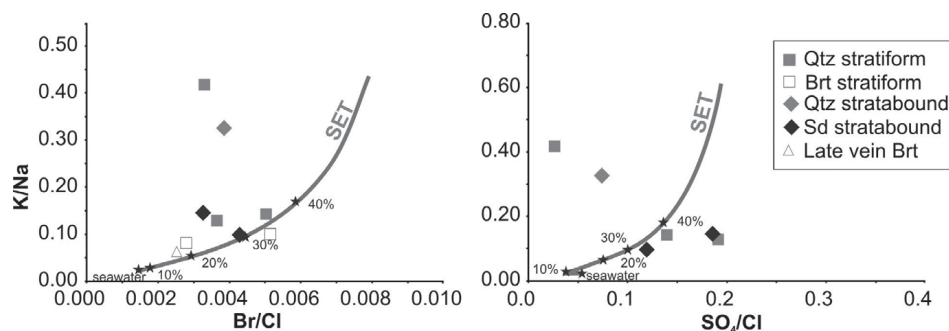


Figure 25: Composition of fluids obtained from bulk crush/leachate ionic chromatography on barite, and detrital quartz from stratiform mineralisation, siderite and quartz from stratabound mineralisation and late stage galena–barite veins from Rude: a) K/Na vs. Br/Cl; b) K/Na vs. SO₄/Cl. Evaporation trend of sea water after McCAFFREY et al., 1987; composition of Permian seawater after HORITA et al., 1991.

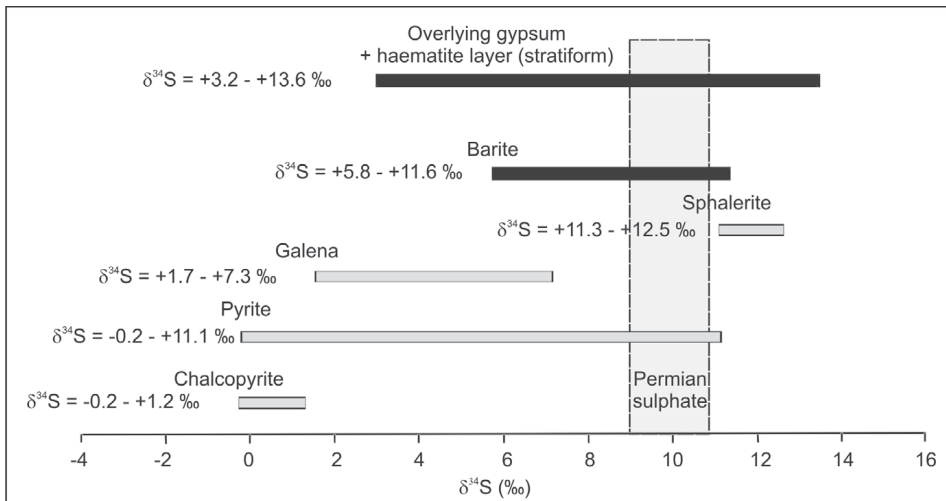


Figure 26: Sulphur isotope data of Cu–Fe–Pb–Zn sulphides, barite and overlying gypsum in relation to Permian sea water sulphates, for explanation see text (CLAYPOOL et al., 1980).

served fluid salinities (max. 20 wt. % NaCl equ.; e.g. under-saturated solution) and the existence of gypsum–anhydrite strata precipitated at 3.8–10.6 % of seawater evaporation. Undersaturation to 20 wt. % NaCl equ. or lower values of salinity were achieved by intrusion of meteoric water, with preservation of the high Br/Cl ratio.

Enrichment of sulphate (SO_4^{2-}/Cl^- ratio) is interpreted as the contribution of an extraneous source, which might have been oxidation of sulphide ions brought by hydrotherms, or from the host black shale by discharge of organically bounded sulphur or dissolution of sedimentary pyrite. Oxidation of sulphide ions is evidenced in lowering of $\delta^{34}S$ values in evaporites to +3 ‰.

As a corollary, the dominant portion of fluid was evaporated seawater, which temporarily did pass the halite precipitation point, and was modified by evolved hydrothermal water and intrusion of meteoric water. The result was spoiling of the SET line, by raising K/Na and increasing the SO_4^{2-}/Cl^- ratio of the fluids.

Detrital quartz in the stratiform mineralisation had a puzzling habit, not corresponding to the common sedimentary origin. The uncommon but ubiquitous jigsaw–fit structure of

the detrital quartz, as well as planar deformation features across the quartz grains, PDFs, (KIEFFER et al., 1976; Figs. 21; 22), provide evidence of two distinctive episodes during formation of the stratiform ore. The first one, responsible for the trails of liquid and solid inclusions across the chert aggregates, is a shock phenomenon (PDFs, high T_h , 150–231 °C, and higher Cl^- concentration; Figs. 21, 22, 24C). The second is sedimentation of massive haematite ore accompanied by barite, documented by their higher sulphate content (ion chromatography data, Table 2), and incorporation of detrital quartz.

According to ŠIFTAR (1989), the $\delta^{34}S$ values of overlying gypsum from Samoborska Gora Mts. are between +3.2 and +13.6 ‰ (Fig. 26, Table 3). Most of the values (between +9 and +11 ‰) fall within the range of Permian marine sulphates (CLAYPOOL et al., 1980). Lower values, between +3 and +7 ‰, are controlled by oxidation of the ascending ore forming fluids, rich in sulphide species. Increased values (up to +13.5 ‰) are interpreted as representing deposition of gypsum from the ascending sulphate already modified by the thermochemical reduction of seawater which produced isotopic light sulphides and fractionated sulphates, heavier than those of the Permian evaporitic water.

These data overlaps with the $\delta^{34}S$ value of sulphates in the barite from the stratiform mineralisation (+6.0 ‰), indicating the strong influence of the Permian seawater sulphate, slightly modified by sulphate formed by oxidation of hydrothermal sulphide.

Isotopic composition of sulphides from the vein mineralisation varies between –0.2 and +12.5 ‰ (Fig. 26). A general trend of increasing isotopic values toward the late stage of mineralisation is observed (chalcopyrite < galena < sphalerite). Maximum values of sulphide overlap with the values within overlying gypsum strata, proposing progressive thermochemical reduction, to completion, of the Permian seawater sulphate. Sulphides did seemingly precipitate under non–equilibrium conditions. The virtual non–equilibrium between sulphate and sulphide within the ore forming fluid, and increasing trend of sulphide isotopes, is a result of successive precipitation from Malcopyrite to sphalerite, with a gradual rise in sulphide isotope composition. Pyrite shows

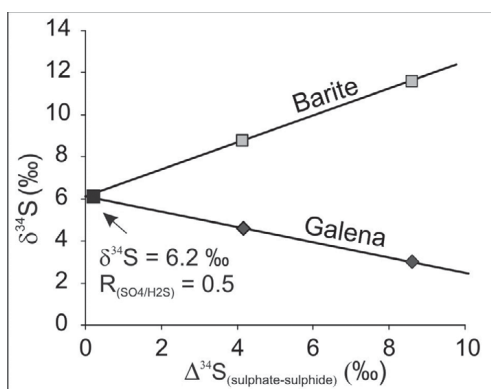


Figure 27. The composition of the sulphur source for the late galena–barite veins was determined on the $\delta^{34}S_{\text{barite/galena}}$ vs. $\Delta^{34}S_{\text{barite-galena}}$ plot. Ore forming fluid from which barite and galena precipitated had $\delta^{34}S_{25}$ value of +6.2 ‰, and the ratio sulphate/sulphide $R_{SO_4/H_2S} = 0.5$, is determined by the slope of the line $\delta^{34}S_{\text{galena}}$ vs. $\Delta^{34}S_{\text{barite-galena}}$.

Table 4: Geochemistry of a selected gypsum sample: a) Major elements (XRF, %); b) trace elements (ICP-MS, ppm), sulphur isotope ($\delta^{34}\text{S}$, ‰); and c) REE (ICP-MS, ppm).

a) Major elements (XRF, %)														
SiO ₂	TiO ₂	Al ₂ O ₃	Fe ₂ O ₃	MnO	MgO	CaO	Na ₂ O	K ₂ O	P ₂ O ₅	SO ₃	Cl	F	LOI	Summ
0.55	0.022	0.33	0.12	0.01	0.26	31.73	0.1	0.06	0.02	44.59	0.004	0.258	21.7	99.76
b) Trace elements (ICP-MS, ppm), sulphur isotope ($\delta^{34}\text{S}$ ‰)														
Ba	Zn	Pb	Cu	Cr	Mn	Ni	Sr	Ti	V	$\delta^{34}\text{S}$ (‰)				
534.0	31.5	258.0	2.1	2.7	17.4	3.4	891.0	57.7	3.4	11.1				
c) REE (ICP-MS, ppm)														
La	Ce	Pr	Nd	Sm	Eu	Gd	Tb	Dy	Ho	Er	Tm	Yb	Lu	
0.580	1.200	0.150	0.570	0.100	0.074	0.093	0.016	0.092	0.018	0.050	0.007	0.058	0.009	

scatter of values in responds to precipitation from the earliest to the latest phases, as Py I, Py II and Py III. The successions are clearly observed by ore microscopy, and progressive replacement stages (Figs. 4 to 20, OHMOTO & RYE, 1979; OHMOTO & LASAGA, 1982).

The composition of the sulphur source for the late galena–barite veins was determined from the isotopic values of galena and barite plotted on the $\delta^{34}\text{S}_{\text{barite/galena}}$ vs. $\Delta^{34}\text{S}_{\text{barite-galena}}$ plot. Ore forming fluid from which barite and galena precipitated had an $\delta^{34}\text{S}_{\text{SS}}$ value of +6.2 ‰ (Fig. 27). The ratio sulphate:sulphide, $R_{\text{SO}_4/\text{H}_2\text{S}} = 0.5$, was determined by the slope of the line $\delta^{34}\text{S}_{\text{galena}}$ vs. $\Delta^{34}\text{S}_{\text{barite-galena}}$.

The sample of gypsum collected at the old hematite mining site of Klassenbruch has a value of +11.1 $\delta^{34}\text{S}$, which approximates to the well known negative peak on the curve of secular variation of Permian sea water. The gypsum sample, on the other hand, has an unusually high lead (258 ppm),

Ba (534 ppm), V (3.4 ppm), Ni (3.4), and Cr (2.1) content (Table 4), which speaks in favour of the contribution of metal rich brines, issuing intermittently into the evaporitic ponds. It was already evidenced by the existence of low sulphate isotope values in some gypsum samples (ŠIFTAR, 1989). High Pb (534 ppm) and the relatively low content of Zn (31.5 ppm) and Cu (2.1 ppm) is due to the low mobility of PbSO_4 , and dissipation of the other two ore metals, which are mobile in a Cl^- and SO_4^{2-} rich environment. Concentrations of REE are highly enriched relative to standard ocean water (SOW) by a factor 10^5 to 10^6 (MARTIN & WITHFIELD, 1983; Fig. 28). The flat, REE diagram, normalized to SOW, supports the open marine origin of evaporating water, with little or no influence from potential dry land run-off (PLAYA et al., 2007). Lack of a negative Ce/Ce* anomaly and positive Eu/Eu* is further evidence of hydrothermal input into the evaporitic ponds.

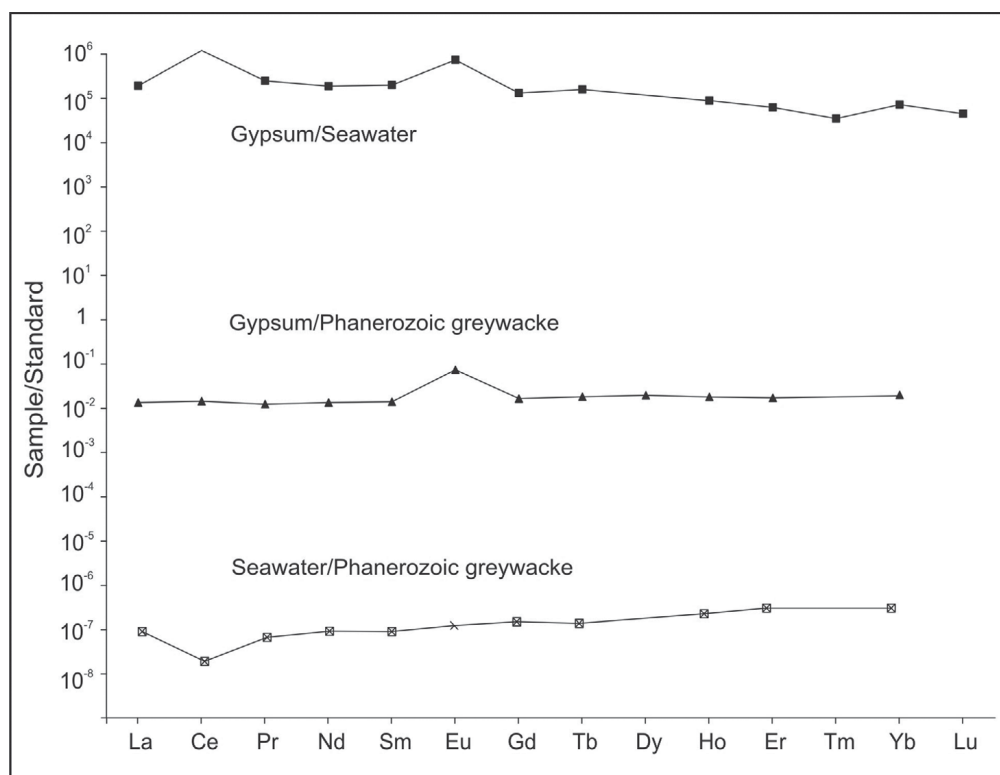


Figure 28: REE in a gypsum sample from the Klassenbruch hematite mining site, normalized to the standard sea water (MARTIN & WHITFIELD, 1983), and Phanerozoic greywacke (TAYLOR & MCLENNAN, 1985). The sea water is also normalized to the greywacke (analyses were undertaken in the Bundesanstalt, Hannover, by V. MARCHIG).

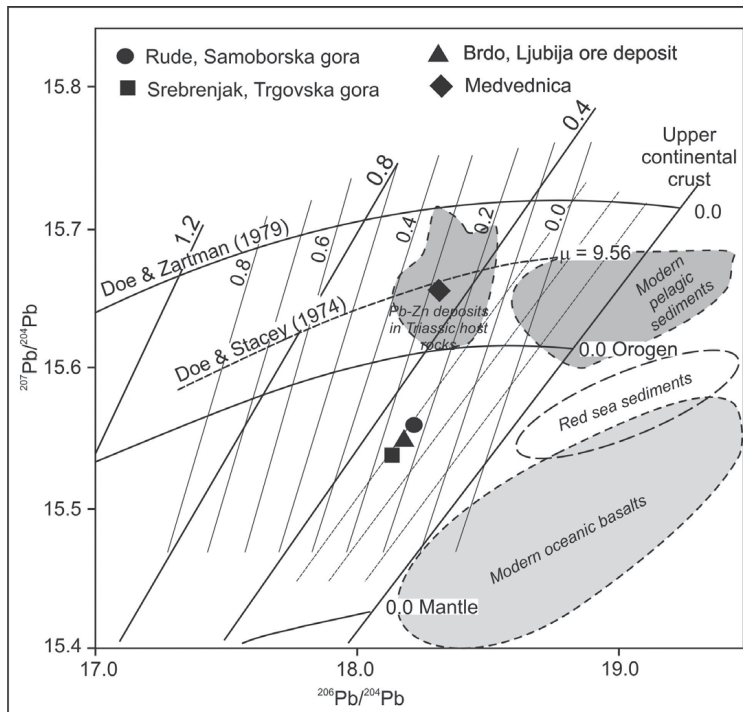


Figure 29: Lead isotope evolution diagram with growth curves according to DOE & STACEY (1974). The curve represents the evolution of the average crustal lead, with an area discriminated for the MORB basalts, Red sea sediments and modern pelagic sediments. DOE & ZARTMAN (1979) growth curves are constructed for the discrete lead reservoirs, in the Upper and Lower Crust and Mantle. Lead isotope data of Permian siderite deposits from the Trgovska Gora Mts., Ljubija and Samoborska Gora Mts. are distinctly separate from the Middle Triassic Pb-Zn deposits in the carbonates (Mežica, Bleiberg, Salafossa, and Sv. Jakob, Medvednica Mts.), between the lead growth curves of Orogen and Mantle (Lower Crust out of the plot).

Lead isotope values obtained on galena from siderite–polysulphide–barite–quartz deposits of Samoborska Gora Mts., Trgovska Gora Mts. and Ljubija, yield coherent model ages of 275, 285 and 280 Ma respectively, by use of isochrones on the DOE–ZARTMAN (1979) multistage growth curves (PALINKAŠ, 1985; 1988). The Pb–isotope evolution diagram with growth curves, (broken curve, $\mu = 9.56$; Fig. 29), represents (according to DOE & STACEY, 1974), the evolution of average crustal lead. The $^{207}\text{Pb}/^{204}\text{Pb} - ^{206}\text{Pb}/^{204}\text{Pb}$ values of the three deposits are marked on the plot and occupy the area between Orogen, Mantle and Lower Crust. The Pb–Zn deposits in Triassic host rocks, Bleiberg–Kreuth, Raibl, Mežica, Salafossa, including Pb–Zn deposit Sv. Jakob on Medvednica, fall in the area marked by the broken line, designating the Upper Crustal reservoir (KÖPPEL, 1983; ZARTMAN & HEINES, 1988). One can distinguish two lead provinces, the Inner Dinarides with siderite–polysulphide–barite–quartz deposits, including Rude, and a younger one with Pb–Zn deposits in carbonates like Bleiberg and Mežica, within the pre-existing Triassic carbonate platform. The lead incorporated in galena of the two distinctly different ore types, originated from the basement greywackes, rich in feldspars (bearer of the common lead) by interaction with mineralizing fluids. The radiogenic Pb–rich source for the Upper Palaeozoic deposits, related to the rifting processes, is placed as shallow, affected by sub–terrestrial hydrothermal cells, flashed by heated evaporitic sea water. In contrast, ore forming fluids for the Triassic Pb–Zn deposits are deep seated brines, remobilized from deeper parts of the Gondwana basement, with older but more radiogenic lead.

The genetic model of the Rude ore deposit had been proposed by Šinkovec (1971) supported by detailed underground and surface geological mapping. The model relies on the geosyncline concept, and field observations, and suggests

the major physical processes engaged in the ore formation. The research presented here, sheds more light on the geochemistry of chemical processes, introducing global tectonic elements in order to establish the model and to answer the unresolved questions regarding tectonic environment, thermal regime, and the source of the metal and sulphur.

The Upper Permian and the P/T boundary, was a transition time between the Early intracontinental and Advanced rifting stages in the formation of Neotethys, as marked by thermal doming and extensional tectonics. Dry land facies, evaporite ponds, a disturbed thermal regime in the incipient rifts, due to rifting magmatism, created favourable ore forming conditions for hydrothermal ore deposits (SEDEX) with a well developed feeder zone in the subterrestrial level. Hydrothermal convective cells along the passive continental margin of Gondwana, demarcating the future opening of the Neotethys, produced numerous siderite–barite–polysulphide deposits in the Alps, Dinarides, Hellenides and Albanides.

Fig. 30 depicts a genetic model with basic physico-chemical processes, which governed the ore formation.

The Rude ore deposit is a SEDEX (volcano–sedimentary) hydrothermal deposit with a genetically linked feeder zone below the stratiform and stratabound ore bodies. The rifting tectonic regime, comprised thermal disturbance, caused by wide–spread magmatic activity, and reaching paroxysm in the Middle Triassic. While the global lateral extension developed deep water rift basins, and subsequent Jurassic oceanization, the early rifting phenomena, including the Rude mineral deposit faded gradually, and their products were covered by the stable Mesozoic carbonate platform compiled of mostly carbonate sediments. The convective hydrothermal cell, forced by volcanism, as *dues ex machine*, (wide–spread but not recorded within the deposit itself), generated ore bearing fluids. The special chemistry of the fluid was com-

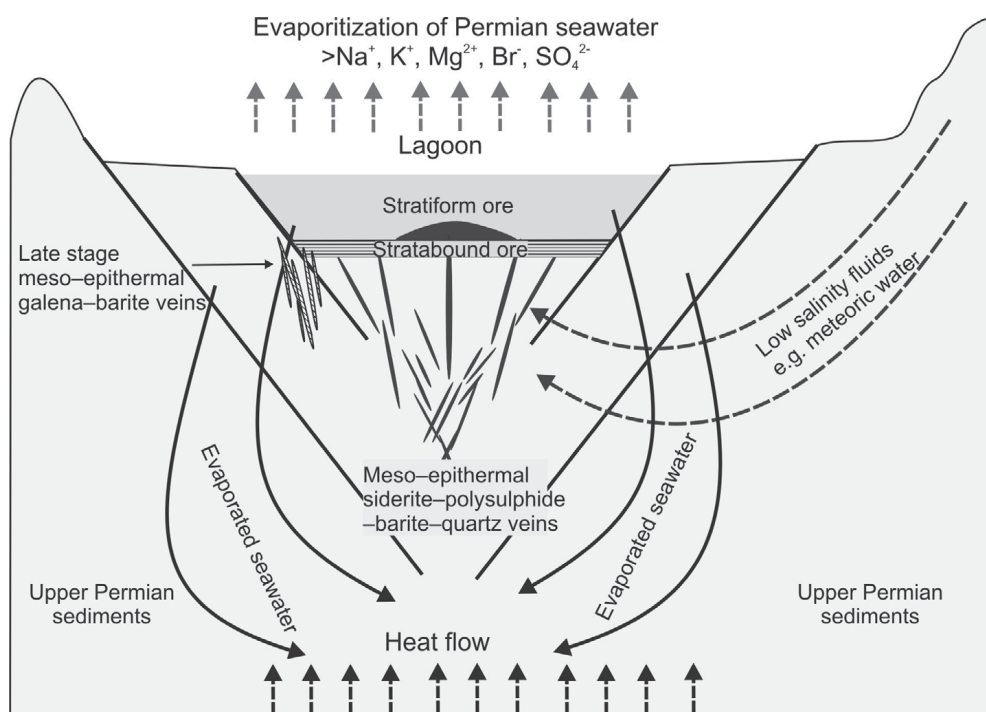


Figure 30: The figure depicts a genetic model with basic physico-chemical processes which governed the ore formation. The Rude ore deposit is a SEDEX (volcano-sedimentary) hydrothermal deposit with genetically linked feeder zone below the stratiform and stratabound ore bodies. The rifting tectonic regime, followed by thermal disturbance, created a subsurface convective circulation of hot brines over thermal anomalies, as *dues ex machine*, generated ore bearing fluids. The fluid chemistry was derived from that of evaporitic brines and meteoric water which sank from the surface into the sub-terrestrial environment below, and interacted with the sedimentary host rocks. Physico-chemical changes of surficial waters include heating, alteration of the redox-potential and pH, leaching of sedimentary sulphur and dispersed metals, upgrading into the ore forming concentration. Precipitation of ore minerals began on the way to the surface in the feeder zone, within the porous sediment below the evaporitic pond, forming stratabound ore bodies. The mineralized water issued into the pond and coprecipitated with evaporites as stratiform ore.

posed of evaporitic brines and meteoric water which sank from the surface into the sub-terrestrial environment and interacted with the sedimentary host rocks. The physico-chemical change of surficial waters includes heating, alteration of redox-potential and pH, leaching of sedimentary sulphur and dispersed metals, while upgrading into the ore forming concentration. Precipitation of ore minerals started on the way to the surface in the feeder zone, within the porous sediment below the evaporitic pond, forming stratabound ore bodies. At the same time the mineralized water issued into the pond and coprecipitated with evaporites as stratiform ore. The impact shock must have been an interregnum event if one ever existed in the ore forming period.

8. CONCLUSION

The Rude deposit in the Samoborska gora Mts. is hosted by Permian non-metamorphosed siliciclastic sediments and evaporates, and composed of stratiform haematite-barite ore, stratabound/vein siderite-polysulphide-barite-quartz mineralisation, and late stage galena-barite veins. Comparative study, of all types of mineralisation, provided a relevant basis for convincing genetic model. Ore forming fluids were formed by a convective hydrothermal cell over thermal anomalies (HARDIE, 1990), caused by wide-spread rifting magmatism (not recorded within the ore deposit itself). Residual evaporitic brines, derived primarily from the Permian seawater, were

involved and modified by interaction with the Late Palaeozoic sedimentary sequence (LEACH et al., 2005). The following evidence and data support the genetic model:

Sulphur isotope composition of overlying gypsum involves Permian seawater sulphate. The sample of gypsum collected at the old haematite mining site of Klassenbruch has a value of +11.1 $\delta^{34}\text{S}$, what approximates to the well known negative peak on the curve of secular variation of sulphur isotopes in the Permian sea water. A wide variation of sulphate isotope values in gypsum, colored by pinkish and brownish hues, from light 3.2 to heavy 13.6 $\delta^{34}\text{S}$ ‰, (a hanging-wall above the stratabound mineralisation), is explained by the introduction of extraneous sulphate by hydrothermal water into the evaporitic ponds. The light sulphate was formed by oxidation of hydrothermal sulphide ions. The heavy isotope ratio was generated by opposite process, reduction of sulphate, which might have been inorganic or organic in origin, and fractionation between sulphide/sulphate.

This data overlaps with the $\delta^{34}\text{S}$ values of sulphates in the barite from the stratiform mineralisation, indicating the strong influence of the Permian seawater sulphate, slightly modified by sulphate formed by oxidation of hydrothermal sulphide.

The vein/stratabound mineralisation precipitated from fluids with highly variable salinities (between 5.3 to 19.2 NaCl equ. wt. %). Homogenisation temperatures of fluid inclusions, which encapsulated ore forming fluids, is between 56 °C and 158 °C.

Late stage barite–galena veins precipitated from moderate salinity–low temperature fluid (salinity between 11.5 and 16.2 NaCl equ. wt.%), which were trapped in fluid inclusions displaying homogenisation temperature between 102 °C and 140 °C. Ore forming fluid, which precipitated barite and galena, had an $\delta^{34}\text{S}_{\text{SS}}$ value of +6.2 ‰, and the ratio sulphate/sulphide $R_{\text{SO}_4/\text{H}_2\text{S}} = 0.5$. Fluid inclusions bulk leachate chemistry recorded the presence of Na^+ , Mg^{2+} , K^+ , Ca^{2+} , Li^+ and Cl^- and SO_4^{2-} ions in the fluids.

The stratiform type of mineralisation precipitated from predominantly Na–Mg–Ca–K chloride solutions. The amount of SO_4^{2-} is increased in haematite samples, due to finely dispersed barite probably (ratio $\text{SO}_4^{2-}/\text{Cl}^-$ from 0.1 to 0.4). Leachate of the haematite samples confirms Mg–K–Ca–Na sulphate rich solution.

The uncommon but ubiquitous jigsaw–fit structure of the detrital quartz, (mostly chert in origin), as well as planar deformation features across the quartz grains, PDFs, (KIEFFER et al., 1976; Figs. 21; 22), provides evidence for a possible shock episode induced by meteorite impact at the P/T boundary, during formation of the stratiform mineralisation.

Isotopic composition of sulphides from the vein mineralisation varies between –0.2 and +12.5 ‰. The sulphur isotopic composition is interpreted as a product of the thermochemical reduction of Permian marine sulphate.

The general trend of increasing isotopic values toward the late stage of mineralisation is as follows: chalcopyrite < galena < sphalerite. The maximum value of sulphur isotopes in sphalerite (+12.5 ‰) overlaps with the values of the overlying gypsum strata, proposing progressive thermochemical reduction to the completion, of the Permian seawater sulphate.

Lead isotope values obtained on galena from Samoborska Gora, Trgovska Gora and Ljubija siderite–polysulphide–barite–quartz deposits yield coherent model ages, 275, 285 and 280 Ma respectively, by using isochrones on the DOE–ZARTMAN (1979) multistage growth curves (PALINKAŠ, 1985; 1988).

Siderite–polysulphide–barite–quartz deposits of Samoborska Gora Mts., Trgovska Gora Mts. and Ljubija are remarkably comparable in geology, mineralogy, geochemistry of fluids and nature of metal sources. Siderite deposits can be easily correlated with similar siderite deposits hosted within non-metamorphosed units of the Inner Dinarides (Ljubija, NW Bosnia), and with those in the Zagorje–Mid–Transdanubian zone. These include; Rudabanya (northernmost Hungary, Lower Triassic), siderite–magnesite–polysulphide deposits in Gemerides (Rudnyani, Nižna Slana, Jelšava and others), and siderite deposits in Eastern Alps (PALINKAŠ et al., 2008; PROCHASKA & HENJES-KUNST, 2007; HURAI et al., 2002; RADVANEC et al., 2004).

The Rude deposits with characteristic geotectonic setting, structural geology, chemistry of ore forming fluids, stable and radiogenic isotope composition of mineral parageneses, represents *locus typicus* of the Permian siderite–barite–polysulphide deposits in the western Tethyan realm.

ACKNOWLEDGEMENT

This paper is a result of a large scale study and research activity under the projects, 119-0982709-1175, 098-0982934-2742 of the Ministry of Science, Education and Sports, Republic of Croatia, and the SCOPES Project No. 7KRPJ065483.01, to whom we express our sincere gratitude. Thanks also go to Tihomir MARJANAC for constructive discussion and relevant literature on the problems of shock quartz and impact phenomena, and to Vesna MARCHIG for geochemical and isotopic data on a gypsum sample, processed in the Bundesanstalt, Hannover. Acknowledgement are also addressed to the reviewer Vesnica GARAŠIĆ and Ferenc MOLNÁR whose comments, suggestions and meticulous reduction greatly cleared up those statements which were taken clear as granted.

REFERENCES

- BASCH, O. (1981): Osnovna geološka karta SFRJ 1:100000, list Ivanić-grad, L 33–81 [*Basic geological map of SFR Yugoslavia scale 1 : 100000, sheet Ivanić-Grad, L 33–81 – in Croatian*].– Inst. geol. istraž., Zagreb, Sav. geol. zavod, Beograd.
- BAKKER, R.J. (2003): Package FLUIDS 1. Computer programs for analysis of fluid inclusion data and for modeling bulk fluid properties.– Chem. Geol., 194, 3–23.
- BOROJEVIĆ ŠOŠTARIĆ, S. (2004): Geneza sideritno-baritno-poli-sulfidnih ležišta u paleozoiku unutarjih Dinarida [*Genesis of the siderite–barite–polysulphide deposits within the Palaeozoic blocks of Inner Dinarides – in Croatian*].– Unpubl. M.Sc. Thesis, University of Zagreb, 120 p.
- BOROJEVIĆ ŠOŠTARIĆ, S., PALINKAŠ L.A., STRMIĆ PALINKAŠ, S., BERMANEC, V., NEUBAUER, F., SPANGENBERG, J. & PROCHASKA, W. (2009): Origin of siderite mineralisations in Petrova and Trgovska Gora Mts., NW Dinarides.– Mineral. Petrol., 97, 111–128.
- BOTTRELL, S.H., YARDLEY, B.W.D. & BUCLEY, F. (1988): A Modified Crush–Leach Method for the Analysis of Fluid Inclusion Electrolytes.– Bull. Mineral., 111, 279–290.
- CHANNER, D.M.DER., BRAY, C.J. & SPOONER, E.T.C. (1999): Integrated cation–anion volatile fluid inclusion analysis by gas and ion chromatography; methodology and examples.– Chem. Geol., 154, 59–82.
- CLAYPOOL, G.E., HOLSER, W.T., KAPLAN, I.R., SAKAI, H. & ZAK, I. (1980): The age curves of sulphur and oxygen isotopes in marine sulphate and their mutual interpretation.– Chem. Geol., 28, 199–260.
- CRAWFORD, M. (1981): Phase equilibria in aqueous fluid inclusions.– In: HOLLISTER, L. & CRAWFORD, M. (eds.): Fluid Inclusions: Applications to Petrology. Mineral. Assoc. Canada Short Course, 6, 304 p.
- CUMMING, G.L. & RICHARDS, J.R. (1975): Ore lead isotope ratios in a continuously changing earth.– Earth Planet. Sci. Lett., 28, 155–171.
- DAVIS, D.W., LOWENSTEIN, T.K. & SPENCER, R.J. (1990): Melting behaviour of fluid inclusions in laboratory–grown halite crystals in the systems NaCl–H₂O, NaCl–KCl–H₂O, NaCl–MgCl₂–H₂O, and NaCl–CaCl₂–H₂O.– Geochim. Cosmochim. Acta, 54, 591–601.
- DOE, B.R. & STACEY, J.S. (1974): The application of lead isotopes to the problems of ore genesis and ore prospect evolution: A review.– Econ. Geol., 63, 757–776.
- DOE, B.R. & ZARTMAN, E. (1979): Plumbotectonics, the Phanerozoic.– In: BARNES, H. L. (ed.): Geochemistry of hydrothermal ore deposits.– John Wiley and Sons, New York, NY, 22–70.
- FRENCH, M.B. (1998): Traces of Catastrophe. LPI contribution No. 954.– Lunar and Planetary Institute, Houston, Texas, 120 p.

- GRIEVE, R.A.F., LANGENHORST, F. & STÖFFLER, D. (1996): Shock metamorphism of quartz in nature and experiment: II Significance in geoscience.– *Meteorites Planet. Sci.*, 31, 6–35.
- HARDIE, L.A. (1990): The roles of rifting and hydrothermal CaCl₂ brines in the origin of potash evaporates: an hypothesis.– *Amer. Jour. Science*, 290, 43–106.
- HERAK, M. (1956): Geologija Samoborskog gorja.– *Acta geol., JAZU, Zagreb*, 1, 49–74.
- HAAS, J., MIOČ, P., PAMIĆ, J., TOMLJENOVIĆ, B., ARKAI, P., BERČZI-MAKK, A., KOROKNAI, B., KOVACS, S. & FELGANHAUER, E. (2000): Complex structural pattern of the Alpine–Dinaric–Pannonian triple junction.– *Int. J. Earth. Sci. (Geol. Rundsch.)*, 89, 377–389.
- HORITA, J., FRIEDMAN, T.J., LAZAR, B. & HOLLAND, H.D. (1991): The composition of Permian seawater.– *Geochim. Cosmochim. Acta*, 55, 417–432.
- HURAI, V., HARCOVA, E., HURAIJOVA, M., OZDN, D., PROCHASKA, W. & WIEGEROVA, V. (2002): Origin of siderite veins in the Western Carpathians – I. P-T-X-δ¹³C-δ¹⁸O relations in ore-forming brines of the Rudnany deposits.– *Ore Geol. Rev.*, 21, 67–101.
- JURKOVIĆ, I. (1958): Metalogeny of Petrova Gora Mts. in southwestern Croatia (in Croatian).– *Geol. vjesnik, Zagreb*, 11, 143–228.
- JURKOVIĆ, I. (1959): Polymetal Paragenesis of the ore occurrence in the catchment area of the Srebrenjak brook south of the town Dvor na Uni in Croatia (in Croatian).– *Geol. vjesnik, Zagreb*, 13, 149–161.
- JURKOVIĆ, I. (1960): Mineralogical Investigation of Iron–ore deposit Ljubija near Prijedor in Bosnia (in Croatian).– *Geol. vjesnik, Zagreb*, 14, 161–220.
- JURKOVIĆ, I. (1961): Minerali željeznih rudnih ležišta Ljubije kod Prijedora [*Mineralogical Investigation of Iron–ore deposit Ljubija near Prijedor in Bosnia* – in Croatian].– *Geol. vjesnik, Zagreb*, 14, 161–220.
- JURKOVIĆ, I. (1962): The results of ore deposit research in Republic of Croatia (in Croatian).– *Geol. vjesnik, Zagreb*, 15/1, 249–294.
- JURKOVIĆ, I. (1988): Hercinska metalogenija rudnih ležišta Trgovske gore u Hrvatskoj [*The Hercynian metallogenesis of the ore deposits of Trgovska Gora in Croatia* – in Croatian].– *Geol. vjesnik, Zagreb*, 41, 369–393.
- JURKOVIĆ, I. & DURN, G. (1988): Lead Deposit in the Zrin District of Trgovska gora in Croatia.– *Geol. vjesnik, Zagreb*, 41, 317–339.
- KIEFFER, S.W. (1971): Shock metamorphism of the Coconino Sandstone at Meteor Crater, Arizona.– *J. Geophys. Res.*, 76, 5449–5473.
- KIEFFER, S.W., PHAKEY, P.P. & CHRISTIE, J.M. (1976): Shock processes in porous quartzite: Transmission electron microscope observations and theory.– *Contr. Mineral. Petrol.*, 59, 41–93.
- KÖPPEL, V. (1983): Summary of lead isotope data from ore deposits of the Eastern and Southern Alps: Some metallogenetic and geotectonic Implications.– In: SCHNEIDER, H.J. (ed.): *Mineral Deposits of the Alps and of the Alpine Epoch in Europe*. Springer–Verlag, Berlin–Heidelberg, 402 p.
- LEACH, D., MARSH, E., BRADLY, D., GARDOLL, S. & HUSTON, D. (2005): The distribution of SEDEX Pb–Zn deposits through Earth history.– In: JINGWEN M. & BIERLEIN F.P. (eds.): *Mineral Deposit Research: Meeting the Global Challenge Proceedings of the Eighth Biennial SGA Meeting Beijing*, 145–148.
- MARTIN, J.M. & WHITFIELD, M. (1983): The significance of the river input of chemical elements to the ocean.– In: WONG, C.S. & BOYL, E. et al. (eds.): *Trace metals in sea water*. Plenum, New York, 265–296.
- McCAFFERY, M.A., LAZAR, B. & HOLLAND, H.D. (1987): The evaporation path of seawater and the coprecipitation of Br and K⁺ with halite.– *J. Sedim. Petrol.*, 57, 928–937.
- MUROWICH, J.B. & BARNES, H.L. (1986): Marcasite precipitation from hydrothermal solution.– *Geochim. Cosmochim. Acta*, 50, 2615–2630.
- NADEN, J. (1996): Calcic Brine: a Microsoft Excel 5.0 Add-in for calculating salinities from microthermometric data in the system NaCl–CaCl₂–H₂O.– In: BROWN, P.E. & HAGEMANN, S.G. (eds.): *PACROFI VI, Pan American Conference on Research on Fluid Inclusion*. Madison Proceedings, 97–98.
- OHMOTO, H. (1986): Stable Isotope Geochemistry of Ore deposits.– In: VALLEY, J.W., TAYLOR, H.P. Jr. & O' NEIL, J.R. (eds.): *Stable Isotopes in High Temperature Geological Processes*. Rev. Mineral., BookCrafters Inc., Chelsea, 16, 419–556.
- OHMOTO, H. & RYE, R.O. (1979): Isotopes of Sulphur and Carbon.– In: BARNES, H.L. (ed.): *Geochemistry of Hydrothermal Ore Deposits*. A Wiley–Interscience publication, New York, 509–561.
- OHMOTO, H. & LASAGA, A.C. (1982): Kinetics of reactions between aqueous sulphates and sulphides in hydrothermal systems.– *Geochim. Cosmochim. Acta*, 46, 1727–1745.
- PALINKAŠ, A.L. (1985): Lead isotopes patterns in galenas from some selected ore deposits in Croatia and NW Bosnia.– *Geol. vjesnik, Zagreb*, 38, 175–189.
- PALINKAŠ, A.L. (1988): Geokemijske karakteristike paleozojskih metalogenetskih terena: Samoborske Gore, Gorskog kotara, Like, Korduna i Banije [*Geochemical characteristics of Palaeozoic metallogenic regions: Samoborska Gora Mts., Gorski kotar, Lika, Kordun and Banija* – in Croatian].– Unpubl. PhD thesis, University of Zagreb, 108 p.
- PALINKAŠ, A.L. (1990): Siderite–barite–polysulphide deposits and Early continental rifting in Dinarides.– *Geol. vjesnik, Zagreb*, 43, 181–185.
- PALINKAŠ, A.L., BOROJEVIĆ, S., STRMIĆ, S., PROCHASKA, W. & SPANGENBERG, J. (2003): Siderite–haematite–barite–polysulphide mineral deposits, related to the Early intra–continental Tethyan rifting, Inner Dinarides.– In: ELIOPOULOS, D.G. et al. (eds.): *Mineral Explorations and Sustainable Development. Proceedings of the 7th Biennial SGA Meeting Athens, Greece, 24–28 August, 2003*, Millpres, Rotterdam, 1225–1228.
- PALINKAŠ, L., BOROJEVIĆ ŠOŠTARIĆ, S. & STRMIĆ PALINKAŠ, S. (2008): Metalogeny of the North–western and Central Dinarides and Southern Tisia.– *Ore Geol. Rev.*, 34, 501–520.
- STRMIĆ PALINKAŠ, S., SPANGENBERG, J. & PALINKAŠ, A.L., (2009): Organic and anorganic geochemistry of Ljubija siderite deposits, NW Bosnia and Herzegovina.– *Miner. Deposita*, 44, 893–913.
- PAMIĆ, J. & TOMLJENOVIĆ, B. (1998): Basic geological data from the Croatian part of the Zagorje–Mid–Transdanubian Zone.– *Acta Geol. Hungarica*, 41/4, 389–400.
- PLAYA, E., CENDON, D.I., TRAVE, A., CHIVAS, A.R. & GARCIA, Y.A. (2007): Using multiple geochemical proxies to trace origin of gypsum (Gulf of Carpentaria, Australia, –70ka).– *Geogaceta*, 42, 135–138.
- PROCHASKA, W. & HENJES-KUNST, F. (2007): The origin of sparry magnesite in the Eastern Alps: evidence from inclusion fluid and Sr–Nd isotope chemistry.– In: ANDREW, C.J. et al. (eds.) *Proceedings of the 9th Biennial Meeting of the Society for Geology applied to Mineral Deposits*. Dublin, IAEG, vol. II, 823–826.
- RADVANEK, M., GREČULA, P. & ŽÁK, K. (2004): Siderite mineralisation of the Gemericum superunit (Western Carpathians, Slovakia): review and a revised genetic model.– *Ore Geol. Rev.*, 24, 267–298.
- RISING, B.A. (1973): Phase relations among pyrite, marcasite and pyrrhotite below 300°C.– Ph.D. dissertation, The Pennsylvania State University, 192 p.

- ROEDDER, E. (1984): Fluid inclusions.– Mineral. Soc. Amer. Rev. Mineral., 12, Washington, 644 p.
- SCHOONEN, M.A.A. & BARNES, H.I. (1991): Mechanism of pyrite and marcasite formation from solution: III. Hydrothermal processes.– Geochim. Cosmochim. Acta, 55, 3491–3504.
- SHEPERD, T.J., RANKIN, A.H. & ALDERTON, D.H.M. (1985): A practical guide to fluid inclusion studies.– Blackie and Son Ltd., Glasgow, 239 p.
- STACEY, J. & KRAMMERS, J.D. (1975): Approximation of terrestrial lead isotope evolution by a two–stage model.– Earth Planet. Sci. Lett., 26, 207–221.
- ŠIFTAR, D. (1989): Starost evaporita i podrijetlo sulfata u Rudama [*The age of evaporates and the origin of sulphate in Rude deposit* – in Croatian].– Geol. vjesnik, Zagreb, 42, 59–64.
- ŠIKIĆ, K., BASCH, O. & ŠIMUNIĆ, A. (1978): Osnovna geološka karta SFRJ 1:100 000. List Zagreb. L33–80 [*Basic geological map of SFRJ 1:100000, Zagreb sheet* – in Croatian].– Inst. geol. istraž., Zagreb (1972), Sav. geol. zavod, Beograd.
- ŠIKIĆ, K., BASCH, O. & ŠIMUNIĆ, A. (1979): Tumač osnovne geološke karte 1:100000, list Zagreb [*Basic geological map of SFRJ 1:100 000, Geology of the Zagreb sheet* – in Croatian].– Sav. geol. zavod, Beograd, 81 p.
- ŠIKIĆ, K. (1995): Geološki vodič Medvednice [*Geological Guide of Medvednica* – in Croatian].– Zagreb: Inst. geol. istraž., Zagreb, 199 p.
- ŠINKOVEC, B. (1971): Geologija ležišta željezne i bakrene rude u Rudama kraj Samobora [*Geology of iron and copper ore from Rude near Samobor* – in Croatian].– Geol. vjesnik, Zagreb, 24, 165–181.
- TAYLOR, S.R. & MCLENNAN, S.M. (1985): The Continental Crust: its Composition and Evolution.– Blackwell Sci. Publ., Oxford, 309 p.
- TOMLJENOVIĆ, B. (2000): Zagorje–Mid–Transdanubian Zone.– In: PAMIĆ, J. & TOMLJENOVIĆ, B. (eds.): Vijesti.– Fieldtrip Guidebook. Proc. of the PANCARDI 2000, Dubrovnik, Croatia, 1–3 October, 2000, Zagreb, 37/2, 27–33.
- TOMLJENOVIĆ, B. (2002): Strukturne karakteristike Medvednice i Samoborskog gorja [*Structural characteristics of the Mts. Medvednica and the Samoborsko Gorje Mts.* – in Croatian].– Unpubl. PhD thesis, University of Zagreb, 208 p.
- ZARTMAN, R.E. & HEINES, S.M. (1988): The plumbotectonic model for Pb isotopic systematics along major terrestrial reservoirs – A case for bi–directional transport.– Geochim. Cosmochim. Acta, 52, 1327–1339.
- ZHANG, Y.G. & FRANTZ, J.D. (1987): Determination of the homogenisation temperatures and densities of supercritical fluids in the system NaCl–KCl–CaCl₂–H₂O using synthetic fluid inclusions.– Chem. Geol., 64, 335–350.

Manuscript received April 15, 2009

Revised manuscript accepted February 10, 2010

Available online February 28, 2010